

WAVEGUIDING AND ELECTROOPTIC MODULATION OF LIGHT  
WITH GaAs EPITAXIAL THIN FILMS

Thesis by  
David B. Hall

In Partial Fulfillment of the Requirements for  
the Degree of  
Doctor of Philosophy

California Institute of Technology  
Pasadena, California

1971

(Submitted May 19, 1971)

Acknowledgments

I wish to express my appreciation to Professor Amnon Yariv and Dr. Elsa Garmire for the invaluable assistance and guidance they gave me during the course of my research.

I would also like to thank the following people: Desmond Armstrong for his skillful assistance in the laboratory; Dr. Allen Shuskus and William Oshinsky of the United Aircraft Research Laboratories for their helpful suggestions and GaAs samples; David Vahey for his aid in the early stages of my research; Paula Samazan for her assistance in the library; and Aldré Khoury, Ruth Stratton, and Karen Current for their job in typing the manuscript.

The financial support received from the Office of Naval Research, Air Force Office of Scientific Research, and the California Institute of Technology is greatly appreciated.

Abstract

Guiding and electrooptic modulation of light at  $1.15\mu$  from a HeNe laser has been achieved in a thin film semiconductor waveguide. The guide was composed of a thin ( $\sim 10\mu$ ) epitaxial film of GaAs sandwiched between a GaAs substrate and an evaporated aluminum coating. The slightly higher refractive index of the guide relative to the substrate allowed the propagation of one single optical TE mode and one single optical TM mode. Large electric fields generated in the epitaxial film by applying a voltage to the aluminum coating, induced an electrooptic change in the refractive index and a consequent modulation of the guided light.

An important new effect, optical mode propagation cut-off, was discovered. Calculations showed that no guided modes propagated below a threshold value of the refractive index difference between guide film and substrate; above that value guiding occurred. This was observed when samples were switched from a non-guiding "off" state to a guiding "on" state by applying a modulation voltage that increased the refractive index of the guide, making it go through cut-off.

Table of Contents

INTRODUCTION	1
1. PROPERTIES OF GaAs	2
1.1 N-type GaAs	2
1.2 Light Propagation in GaAs	3
1.3 Electrooptic Effect	6
1.4 Franz-Keldysh Effect	8
2. EPITAXIAL WAVEGUIDE	11
2.1 Index Profile	11
2.2 Guided Wave Solutions	13
2.3 Comparison of Metal and Air Bound Waveguides	24
3. METAL-SEMICONDUCTOR JUNCTION	29
3.1 Surface States	29
3.2 Schottky Barrier	30
3.3 Barrier Capacitance	33
3.4 Barrier Current	34
4. ELECTROOPTIC WAVEGUIDE MODULATOR	37
4.1 Index Profile	37
4.2 Guided Wave Solutions	38
4.3 Electrooptic Switching	43
4.4 Physical Significance of Cutoff	48
4.5 Intensity Modulation	49
5. THE EXPERIMENTS	55
5.1 Sample Preparation	55

5.	THE EXPERIMENTS (cont)	
5.2	Modulator Setup	56
5.3	Detection Schemes	59
6.	EXPERIMENTAL RESULTS AND INTERPRETATIONS	61
6.1	Intensity Profiles	61
6.2	Optical Cutoff Data	63
6.3	Intensity Modulation Data	69
	FIGURES	73
	REFERENCES	97

Introduction

The recent availability of electrooptic semiconductors such as GaAs with relatively low doping levels ( $10^{15}$  cm<sup>-3</sup>) makes possible for the first time optical waveguiding and modulation in semiconductor epitaxial films. Waveguiding without modulation has been performed in a variety of thin film devices. Recent ones have used high index films deposited on glass substrates and special light input couplers to maximize the amount of waveguided light.<sup>(1,2)</sup> On the other hand, electrooptic modulation has usually been done with bulk crystal modulators.<sup>(3)</sup>

Combining the two operations of waveguiding and electrooptic modulation has been previously accomplished in GaAs and GaP p-n junctions.<sup>(4,5,6)</sup> The junction region with a slightly higher refractive index than the adjacent p and n regions acts as a thin film guide. It propagates guided light which is modulated when a reverse biasing voltage is applied. The chief limitation of the p-n junction modulator is its small length. Better performance is possible in an epitaxial modulator because much larger homogeneous samples can be grown. The optical properties of the epitaxial modulator are controlled by varying the thickness and doping of the epitaxial film and the substrate.<sup>(7,8)</sup>

In this thesis, waveguiding and electrooptic modulation in a number of different epitaxial structures is explored. The first four chapters develop the electrooptic waveguide model used to explain the experimental results of the last two. The propagation of single mode light and its modulation by means of a Schottky barrier space charge layer in the epitaxial film is analyzed and observed. The most important new development is the electrooptic switching of waveguided light covered in Chapters 4 and 6.

Chapter 1

Properties of GaAs

1.1 N-type GaAs

The modulator consists of an epitaxial film of the n-type GaAs deposited on the (100) face of an n-type GaAs substrate. The substrate, doped with either tellurium or silicon, has shallow donor levels .003 or .002 eV below the conduction band edge.<sup>(9)</sup> These energies are much smaller than  $kT$  (.026 eV at  $T = 300^\circ\text{K}$ ), so the donor levels are ionized and the material is extrinsic with a free electron carrier density in the conduction band nearly equal to the donor concentration. The epitaxial material has no external dopants added, but is also extrinsic n-type through residual impurities like silicon.<sup>(10)</sup> The free carrier densities range between  $8 \times 10^{15} \text{ cm}^{-3}$  and  $10^{17} \text{ cm}^{-3}$  for different substrates and average  $10^{15} \text{ cm}^{-3}$  in the epitaxial layer.

The energy gap is 1.43 eV at  $300^\circ\text{K}$ , and the Fermi level lies a few  $kT$  below the conduction band edge. For the lightly doped, non-degenerate material used:

$$E_C - E_F = kT \ln [N_C/N_D] \quad (9) \quad (1-1)$$

$E_C$  Bottom of conduction band

$E_F$  Fermi level

$N_D$  Donor density

$N_C$  Effective density of states in conduction band

$$N_C = 4.7 \times 10^{17} \text{ cm}^{-3} \text{ at } T = 300^\circ\text{K}$$

$$\text{Substrate } N_D = 5 \times 10^{16} \text{ cm}^{-3}, E_C - E_F = .06\text{eV} \sim 2kT \quad (1-2)$$

$$\text{Epitaxial Film } N_D = 10^{15} \text{ cm}^{-3}, E_C - E_F = .16\text{eV} \sim 6kT \quad (1-3)$$

## 1.2 Light Propagation in GaAs

N-type GaAs is more or less transparent to light propagation from the fundamental absorption edge at  $.9\mu$  out to the first lattice absorption band at  $18\mu$ .<sup>(11)</sup> As shown in Figure I, the principal contribution to absorption at wavelengths less than the three micron minimum is due to transitions of electrons from the principal conduction band minimum at  $k = 0$  to higher minima of the same band. Beyond three microns, free carrier absorption is dominant with a  $\lambda^3$  dependence.<sup>(12)</sup> At  $\lambda_0 = 1.15\mu$  the wavelength for modulator operation of the free carrier part is less than 10% and material with  $10^{15} \text{ cm}^{-3}$  conduction electrons has an absorption somewhere between  $.2$  and  $2 \text{ cm}^{-1}$ .<sup>(12,13,14)</sup>

Increasing the doping and hence the number of conduction band electrons in the vicinity of the  $k = 0$  principal minimum enhances absorption. More free electrons are available for scattering into higher minima and for free carrier absorption at longer wavelengths.

The index of refraction is plotted as a function of photon energy in Figure II.<sup>(15)</sup> Unlike absorption which is strongly influenced by the number of free carriers, the index is so insensitive to the carrier number that the effect cannot be measured. However, absorption and index are related through the Kramers-Kronig dispersion relation, and a change in the absorption through a change in the free

carrier concentration should effect a small change in the index.

Looking at the epitaxial modulator for a moment, if the substrate absorption coefficient  $\alpha_3(\lambda)$  and the epitaxial film absorption coefficient  $\alpha_2(\lambda)$  are known for all wavelengths, the change in index  $n_3(\lambda_0) - n_2(\lambda_0)$  in going from epitaxial film to substrate can be determined at  $\lambda_0 = 1.15\mu$ .

$$n_3(\lambda_0) - n_2(\lambda_0) = \frac{\lambda_0^2}{2\pi} \int_0^{\infty} \frac{\alpha_3(\lambda) - \alpha_2(\lambda)}{\lambda_0^2 - \lambda^2} d\lambda \quad (16) \quad (1-4)$$

The substrate is more heavily doped than the epitaxial film so  $\alpha_3(\lambda)$  is larger than  $\alpha_2(\lambda)$ . For wavelengths longer than  $\lambda_0$ , free carrier absorption dominates and gives a negative contribution to  $n_3(\lambda) - n_2(\lambda)$  which is called the free carrier depression of the refractive index.

This sort of analysis has been performed on p-type GaAs for wavelengths shorter than  $.95\mu$  near the band edge, but as far as is known, not for n-type GaAs at  $1.15\mu$ .<sup>(17)</sup> P-type material is more complicated because it has a heavy hole and a light hole valence band which are degenerate at the  $k = 0$  band maximum where intraband and interband scattering of free carrier holes takes place for free carrier optical absorption. N-type material does not have degenerate conduction bands, therefore it does not have an interband contribution to free carrier absorption. Eliminating the interband contribution, the p-type material has a free carrier contribution that amounts to 70% of the total index change at  $.90\mu$ . At  $1.15\mu$ , further away from the absorption edge the free carrier depression of the index is a larger percentage for the p-type material.

An analysis of n-type material would yield similar results and the free carrier depression contribution is probably 90% or more of the total at 1.15 $\mu$ .

A simple model of a free electron gas of density N can be used to illustrate free carrier depression of the index. An AC electric field polarizes the free carriers, contributing to the electric susceptibility of the medium.

$$m^* \ddot{x} = - e E_0 e^{i\omega t} \quad (1-5)$$

$$P = - N e x \quad (1-6)$$

$$\chi_c = P/E = - Ne^2/m^* \omega^2 \quad (1-7)$$

$\chi_c$  is the electric susceptibility of the free carriers and  $m^*$  is the effective mass which is 7.8% of the free electron mass in lightly doped GaAs. (13)

Susceptibility is related to the change in index. At optical frequencies sufficiently far away from any absorption band:

$$\frac{\chi_c}{\epsilon_0} = 2 n \Delta n \quad (1-8)$$

In n-type GaAs where the free electron density is equal to the donor density  $N_D$  :

$$\Delta n = \frac{-1}{2n\epsilon_0} \frac{N_D e^2}{m^* \omega^2} \quad (1-9)$$

$$\Delta n = - 9.6 \times 10^{-21} \frac{N_D}{nE^2} \quad (17) \quad (1-10)$$

$E = \hbar\omega$  is the photon energy in electron volts. The substrate has a much greater number of free electrons than the epitaxial film giving it the lower refractive index.

$$\begin{aligned} \text{Substrate } N_D &= 5 \times 10^{16} \text{ cm}^{-3} \\ \lambda_0 &= 1.15\mu, \quad E = 1.08 \text{ eV}, \quad n = 3.45 \\ \Delta n &= -1.2 \times 10^{-4} \end{aligned} \tag{1-11}$$

This is about the magnitude of  $\Delta n$  necessary for light confinement in the waveguides used in our experiments.

### 1.3 Electrooptic Effect in GaAs

GaAs is an isotropic crystal to light propagation in the absence of an external electric field. The field changes the ionic and electronic polarizability, so the crystal becomes biaxial with various changes in the refractive index along certain crystal axes being proportional to the external field. This behavior is called the linear electrooptic effect.

Optical properties of an anisotropic crystal are described in terms of an index ellipsoid.

$$\frac{x^2}{n_x^2} + \frac{y^2}{n_y^2} + \frac{z^2}{n_z^2} = 1 \tag{18} \tag{1-12}$$

The principal axes are  $x, y,$  and  $z;$  and the refractive indices of light polarized along these axes are  $n_x, n_y,$  and  $n_z.$  In zero external field the index ellipsoid of GaAs is a sphere. When a field  $E$  is turned on the sphere is distorted and becomes:

$$\frac{x^2 + y^2 + z^2}{n_0^2} + 2r_{41} [yzE_x + zxE_y + xyE_z] = 1 \tag{1-13}$$

The electrooptic coefficient  $r_{41}$  produces cross terms which are removed by diagonalizing and finding a set of principal axes. Light traveling along one of the principal axes is composed of two components polarized along the other two axes.

In the modulator, an external DC field is applied at right angles to a (100) crystal plane upon which the aluminum electrode is evaporated.

$$E_x = E_{DC} \quad [100] \text{ direction} \quad (1-14)$$

$$\frac{x^2 + y^2 + z^2}{n_o^2} + 2r_{41} yzE_{DC} = 1 \quad (1-15)$$

Diagonalizing, we obtain:

$$\begin{aligned} \left[ \frac{1}{n_o^2} \right] x'^2 + \left[ \frac{1}{n_o^2} + r_{41} E_{DC} \right] y'^2 \\ + \left[ \frac{1}{n_o^2} - r_{41} E_{DC} \right] z'^2 = 1 \end{aligned} \quad (1-16)$$

$$x' = x \quad [100] \quad (1-17)$$

$$y' = \frac{1}{\sqrt{2}} (y+z) \quad [011] \quad (1-18)$$

$$z' = \frac{1}{\sqrt{2}} (y-z) \quad [0\bar{1}1] \quad (1-19)$$

The principal indices of refraction are:

$$n'_x = n_o \quad (1-20)$$

$$n'_y = n_o - \frac{1}{2} n_o^3 r_{41} E_{DC} \quad (1-21)$$

$$n'_z = n_o + \frac{1}{2} n_o^3 r_{41} E_{DC} \quad (1-22)$$

The electrooptic coefficient  $r_{41}$  is nearly independent of the optical wavelength and has been measured with an error  $\sim 15\%$ . For operation at  $\lambda_o = 1.15\mu$  we have:

$$r_{41} \approx 1.3 \times 10^{-10} \text{ cm/V} \quad (19,20) \quad (1-23)$$

$$n_o^3 r_{41} \approx 5.3 \times 10^{-9} \text{ cm/V} \quad (1-24)$$

From equations 1-21 and 1-22, we obtain:

$$\Delta n_{EO} = \pm \frac{1}{2} n_o^3 r_{41} E_{DC} \quad (1-25)$$

Fields of about  $10^5$  V/cm are attained inside the epitaxial film of the modulator causing index changes larger than  $10^{-4}$ .

$$E_{DC} = 10^5 \text{ V/cm} \quad (1-26)$$

$$\Delta n_{EO} = \pm 2.6 \times 10^{-4} \quad (1-27)$$

The electrooptic index shift is comparable to or larger than the built in index difference between the substrate and the epitaxial film discussed at the end of section 1.2.

#### 1.4 Franz-Keldysh Effect

Another contribution to  $\Delta n$  from an external field occurs for light at photon energies somewhat below the band gap energy  $E_g$ . In an ideal semiconductor, the absorption edge is sharp and there is no

absorption for  $\hbar\omega < E_g$ . An external field blurs the absorption edge, and an exponential absorption tail due to field assisted tunneling extends into the gap, lowering  $E_g$ .<sup>(21)</sup> This is the, so called, Franz-Keldysh effect.

This energy shift of the absorption edge to lower energies has been observed in GaAs, with a square dependence on the external electric field.

$$\Delta E_g = 8 \times 10^{-12} E^2 \quad (22) \quad (1-28)$$

where  $\Delta E_g$  is in eV and E in V/cm. For a field of 5000 V/cm, the highest attained:

$$\Delta E_g = 2 \times 10^{-4} \text{ eV} \quad (1-29)$$

The absorption edge shift should make small changes in the index for wavelengths somewhat longer than  $hc/E_g$  which is about  $.85\mu$ . At a field of 5000 V/cm this was seen when light was sent through a bulk GaAs modulator.<sup>(23)</sup> For wavelengths from  $.85\mu$  to  $.95\mu$ , a large deviation from the normal linear electrooptic behavior was observed in the transmitted light. This deviation was presumably generated by the Franz-Keldysh effect. Beyond  $.95\mu$  the deviation was too small to be detected.

At fields much greater than 5000 V/cm, the Franz Keldysh effect could perhaps induce refractive index changes as far out as  $1.15\mu$ . Calculations for GaAs have been done that indicate an increase in the index for very high fields that is independent of the field direction.<sup>(21)</sup> At  $\lambda_0 = 1.15\mu$  and  $E = 10^6$  V/cm we have:

$$\Delta n = 3 \times 10^{-3} \quad (1-30)$$

No experiment has been done at  $10^6$  V/cm for light transmission through GaAs. However, at fields about 10% as large, index shifts of this nature were not seen when  $1.15\mu$  light was propagated along a reverse biased GaAs p-n junction waveguide modulator.<sup>(5)</sup> At all fields up to  $10^5$  V/cm, the modulation was caused by the linear electrooptic effect.

The epitaxial modulator operates with fields up to  $2 \times 10^5$  V/cm. Therefore, the Franz-Keldysh effect does not significantly modify the linear electrooptic behavior at  $1.15\mu$  for the epitaxial modulator.

## Chapter 2

### Epitaxial Waveguide

#### 2.1 Index Profile

Free electron carriers are used to control the refractive index difference between the epitaxial guide and substrate. The much higher doping of the substrate depresses its index with respect to the guiding layer, permitting light confinement and wave guiding to occur.

The waveguide configuration and index profile are shown in Figure III. The optical wave propagates in the  $z$  direction along the guide which is assumed to extend infinitely in the  $y$  direction. The guide has a thickness  $t$  in the  $x$  direction and is bounded by the aluminum coating at  $x = 0$  and the substrate at  $x = t$ . GaAs has a small optical loss which is ignored in this waveguide model; therefore  $n_2$  and  $n_3$  are taken as real.

On the other hand, the aluminum coating is a strong absorber, so index  $n_1$  is a complex quantity.

$$n_1 = n - ik \quad (2-1)$$

An optical plane wave normally incident on the aluminum is reflected. The reflectance in air is:

$$R = \frac{(n - 1)^2 + k^2}{(n + 1)^2 + k^2} \quad (24) \quad (2-2)$$

At angles other than normal incidence,  $R$  is given by more complicated

formulas. Reflectance data are the most common way of determining  $n$  and  $k$  for metals. For aluminum at  $1.15\mu$ :

$$n_1 = 1.5 - 10i \quad (25) \quad (2-3)$$

Other metals like gold and silver have similar indices at  $1.15\mu$  with the imaginary part much larger than the real part. These numbers are not very precise. They are influenced by film evaporation rate, film thickness, aging in air, and a host of other factors. However, even if the numbers are off by a factor of two, the guided wave solutions are hardly affected. The important factor is the large imaginary part and the small real part of the complex index.

Light incident on the aluminum attenuates exponentially within the aluminum. For normal incidence, the  $1/e$  depth for optical power is:

$$d = \frac{\lambda}{4\pi k} \quad (24) \quad (2-4)$$

At optical frequencies, this distance is extremely small. At  $\lambda_0 = 1.15\mu$ :

$$d = 90\text{\AA} \quad (2-5)$$

The aluminum coating used in the experiment has a thickness many times this number, and the amount of light penetrating it to reach the air interface on the other side is negligible. Consequently, the aluminum layer can be treated as extending to infinity in the  $x$  direction in Figure III.

The guided modes also propagate when the epitaxial guide is in direct contact with the air. In this case, the complex index of

refraction  $n_1$  in Figure III is replaced by  $n_1 = 1$ . An interesting point, which will be discussed in section 2.2, is that solutions are essentially the same for guided modes in both the metal and air bounded waveguides.

## 2.2 Guided Wave Solutions

Referring to Figure III, an optical wave propagating along the epitaxial film in the  $z$  direction is taken as:

$$\vec{E}(x,y,z,t) = \vec{E}(x) \exp[i(\omega t - \beta z)] \quad (2-6)$$

There is no functional dependence on  $y$  since the guide is infinitely extended along  $y$ . Maxwell's equations are separable into two independent sets of solutions; transverse electric (TE) and transverse magnetic (TM) in a rectangular guide.<sup>(26)</sup>

$$\text{TE} \quad E_y, H_x, H_z \quad \text{all} \neq 0 \quad (2-7)$$

$$\text{TM} \quad H_y, E_x, E_z \quad \text{all} \neq 0 \quad (2-8)$$

Let us consider the TE modes first:

$$E_y = E_y(x) \exp[i(\omega t - \beta z)] \quad (2-9)$$

The solutions are:

$$0 < x \quad E_y(x) = A \exp[qx] \quad (2-10)$$

$$0 < x < t \quad E_y(x) = B \exp[ihx] + C \exp[-ihx] \quad (2-11)$$

$$x > t \quad E_y(x) = D \exp[-p(x-t)] \quad (2-12)$$

The propagation constant  $\beta$  in equation (2-9) is complex because losses in the aluminum will cause the TE wave to attenuate as it propagates along the guide. This in turn, makes  $q$ ,  $h$ , and  $p$  complex. However, the imaginary parts as seen later are very small, and the field will have a sinusoidal  $x$  dependence inside the guide and will decay exponentially in the adjacent regions. At the  $x = 0$  and  $x = t$  interfaces, the tangential electric field  $E_y$  is continuous.

$$x = 0 \quad A = B + C \quad (2-13)$$

$$x = t \quad B \exp[iht] + C \exp[-iht] = D \quad (2-14)$$

The magnetic field is connected to  $E_y$  through the curl equation:

$$\nabla \times \vec{E} = -\mu_0 \frac{\partial \vec{H}}{\partial t} \quad (2-15)$$

$$\frac{\partial E_y}{\partial x} = -i\omega\mu_0 H_z \quad (2-16)$$

The tangential magnetic field  $H_z$  is also continuous at the  $x = 0$  and  $x = t$  interfaces, making  $\partial E_y / \partial x$  continuous.

$$x = 0 \quad qA = ihB - ihC \quad (2-17)$$

$$x = t \quad ihB \exp[iht] - ihC \exp[-iht] = -pD \quad (2-18)$$

The four boundary conditions 2-13, 2-14, 2-17, and 2-18 can be expressed as a determinant in  $q$ ,  $h$ , and  $p$  which must equal zero to give the coefficients  $A, B, C$ , and  $D$  non-zero values:

$$\begin{vmatrix} -1 & 1 & 1 & 0 \\ -q & ih & -ih & 0 \\ 0 & e^{iht} & e^{-iht} & -1 \\ 0 & ihe^{iht} & -ihe^{-iht} & p \end{vmatrix} = 0 \quad (2-19)$$

The determinant reduces to:

$$ht = \tan^{-1}(q/h) + \tan^{-1}(p/h) \quad (2-20)$$

This is the first of three equations involving q, h, and p for the TE modes. The other two are obtained from the wave equation:

$$\frac{\partial^2 E_y}{\partial x^2} + [n^2 \left(\frac{\omega}{c}\right)^2 - \beta^2] E_y = 0 \quad (2-21)$$

$$\frac{\omega}{c} = \frac{2\pi}{\lambda_0} \quad (2-22)$$

Substituting the TE fields from 2-10, 2-11, and 2-12 into the wave equation, we have:

$$x < 0 \quad \beta^2 = n_1^2 \left(\frac{2\pi}{\lambda_0}\right)^2 + q^2 \quad (2-23)$$

$$0 < x < t \quad \beta^2 = n_2^2 \left(\frac{2\pi}{\lambda_0}\right)^2 - h^2 \quad (2-24)$$

$$x > t \quad \beta^2 = n_3^2 \left(\frac{2\pi}{\lambda_0}\right)^2 + p^2 \quad (2-25)$$

Eliminating  $\beta$ , we obtain:

$$q^2 + h^2 = [n_2^2 - n_1^2] \left(\frac{2\pi}{\lambda_0}\right)^2 \quad (2-26)$$

$$h^2 + p^2 = [n_2^2 - n_3^2] \left(\frac{2\pi}{\lambda_0}\right)^2 \quad (2-27)$$

which together with 2-20 can be used to solve for q, h, and p.

A similar analysis is used for TM modes in which  $H_y$  replaces  $E_y$ . The procedures coincide except for the boundary conditions 2-17 and 2-18. At  $x = 0$  and  $x = t$ , the tangential magnetic field  $H_y$  is continuous, but its first derivative  $\partial H_y / \partial x$  is not.  $H_y$  is connected to the electric field through the curl equation:

$$\nabla \times \vec{H} = n^2 \epsilon_0 \frac{\partial E}{\partial t} \quad (2-28)$$

$$\frac{\partial H_y}{\partial x} = i\omega n^2 \epsilon_0 E_z \quad (2-29)$$

The tangential electric field  $E_z$  is continuous, making  $1/n^2 \partial H_y / \partial x$  continuous at  $x = 0$  and  $x = t$ . This modification changes the transcendental equation 2-20 in q, h, and p.

For the TM modes, we have:

$$ht = \tan^{-1} \left[ \left(\frac{n_2}{n_1}\right)^2 q/h \right] + \tan^{-1} \left[ \left(\frac{n_2}{n_3}\right)^2 p/h \right] \quad (2-30)$$

We now have the four relations 2-20, 2-26, 2-27, and 2-30 involving q, h, and p for the TE and TM modes. Equations 2-26 and 2-27 apply to both the TE and TM modes, 2-20 applies to just the TE modes, and 2-30 to just the TM modes.

Equations 2-26 and 2-27 can be simplified because the refractive index  $\Delta n = n_2 - n_3$  between the substrate and epitaxial layer is extremely small. From equation 1-11 in section 1.2, it is approximately  $10^{-4}$ . We see that the magnitude of  $n_2^2 - n_3^2$  in 2-26 is very much

larger than the magnitude of  $n_2^2 - n_3^2$  in 2-27 which can be set equal to  $2n_2\Delta n$ . This in turn makes  $|q^2|$  very much larger than  $|h^2|$  and  $|p^2|$ . The simplified equations are:

$$q^2 t^2 \approx [n_2^2 - n_1^2] \left(\frac{2\pi}{\lambda_0}\right)^2 t^2 \quad (2-31)$$

$$(h^2 + p^2) t^2 \approx 2n_2\Delta n \left(\frac{2\pi}{\lambda_0}\right)^2 t^2 \quad (2-32)$$

Referring to Figure III, the  $1/e$  point of field penetration into the metal for  $x < 0$  is  $1/\text{Re}(q)$ . Equation 2-31 states that this penetration is only a function of indices  $n_1$  and  $n_2$ , and is independent of  $h$  and  $p$ .

The two transcendental relations 2-20 for the TE modes and 2-30 for the TM modes can also be modified. The arguments  $q/h$  in 2-20 and  $\left(\frac{n_2}{n_1}\right)^2 q/h$  in 2-30 are both complex. Operating with a wavelength of  $1.15\mu$ ,  $n_2 = 3.45$  from 1-11 and  $n_1 = 1.5 - 10i$  from 2-3. Substituting these values into 2-31, we obtain:

$$q \approx [57 + 8i] (\text{micron})^{-1} \quad (2-33)$$

An upper bound on the size of  $h$  is set by equation 2-32. We assume that  $\Delta n = 10^{-4}$ , and that  $p$  and  $h$  are real. We obtain:

$$h \leq .14 (\text{micron})^{-1} \quad (2-34)$$

The above conditions on  $h$  and  $q$  give the following inequalities for the arguments in 2-20 and 2-30:

$$\frac{q}{h} \approx 400 + 60i \quad (2-35)$$

$$\left(\frac{n_2}{n_1}\right)^2 \frac{q}{h} \approx 40 - 5.5i \quad (2-36)$$

The limiting value of an arc tangent whose argument has a magnitude much larger than one is  $(m + \frac{1}{2})\pi$  for  $m = 0, 1, 2, \dots$ . Using this approximation and the approximation that  $(n_2/n_3)^2 \approx 1$ , transcendental equations 2-20 and 2-30 are simplified. They both give:

$$ht = \tan^{-1}(p/h) + (m + \frac{1}{2})\pi \quad m = 0, 1, 2, \dots \quad (2-37)$$

which can also be expressed as

$$pt = -ht \cot(ht) \quad (2-38)$$

We now have the three relations 2-31, 2-32, and 2-38 involving  $q$ ,  $h$ , and  $p$  for both the TE and TM modes. Equation 2-31 involves  $q$  only, and 2-32 and 2-38 involve just  $h$  and  $p$ .

Before solving for  $q$ ,  $h$ , and  $p$ , let us go back to equation 2-11 that gives  $E_y(x)$  for  $0 < x < t$  for the TE modes. Using boundary conditions 2-13 and 2-17 for  $E_y$  and  $\partial E_y / \partial x$  at  $x = 0$ , we eliminate  $B$  and  $C$ . Now we have:

$$0 < x < t \quad E_y(x) \sim \sin(hx) + \frac{h}{q} \cos(hx) \quad (2-39)$$

A similar analysis for  $H_y(x)$  of the TM modes gives:

$$0 < x < t \quad H_y(x) \sim \sin(hx) + \left(\frac{n_1}{n_2}\right)^2 \frac{h}{q} \cos(hx) \quad (2-40)$$

From conditions 2-35 and 2-36, we see that the second term in both 2-39 and 2-40 is very much smaller than the first term. To a high degree of approximation, the field has the following  $x$  dependence for both the TE and TM modes:

$$0 < x < t \quad E_y(x), H_y(x) \sim \sin(hx) \quad (2-41)$$

In this limit, the field goes to zero at the metal-guide interface at  $x = 0$ . Matching  $E_y(x)$  or  $H_y(x)$  on either side of the guide-substrate interface at  $x = t$ , we obtain:

$$x > t \quad E_y(x), H_y(x) \sim \sin(ht) \exp[-p(x - t)] \quad (2-42)$$

With  $n_2 \approx n_3$ , the first derivatives of both  $E_y(x)$  and  $H_y(x)$  are also matched at  $x = t$ . This yields relation 2-38 in  $h$  and  $p$  that was previously derived from transcendental equations 2-20 and 2-30.

We now see that equations 2-32 and 2-38 involving  $h$  and  $p$  are to be used in the limiting case in which  $n_2 - n_3 \ll 1$  and in which the fields approach zero at the metal-guide interface. In Figure IV is shown a plot of  $pt$  as a function of  $ht$  for equation 2-32 and 2-38. Only positive values of  $pt$  which give decaying exponential solutions of the field for  $x > t$  are considered. For guiding to occur,  $pt$  must be greater than zero. Three circles represent solutions to 2-32 with radii proportional to the square root of  $\Delta n$ ;  $\Delta n$  has to be greater than zero or the radii would be imaginary. Three solid curves crossing the abscissa at  $ht = \pi/2, 3\pi/2, \text{ and } 5\pi/2$  respectively represent multiple solutions to 2-38. The smallest circle does

not intersect any of the curves for 2-38; therefore its value of  $\Delta n$  is too small for a guided mode. The middle circle crosses the  $\pi/2$  curve, and the intersection point is a solution in  $ht$  and  $pt$  for the lowest order  $TE_1(TM_1)$  mode. The largest circle crosses twice; one point is a solution of the lowest order  $TE_1(TM_1)$  mode, and the other of the second lowest  $TE_3(TM_3)$  mode. (The notation will become clearer later on.) The most important feature is the cutoff point of  $\Delta n$  for guiding. No guiding occurs unless the radius of a circle in Figure IV is greater than  $\pi/2$ . Substituting  $ht \geq \pi/2$  and  $pt = 0$  into equation 2-32, we obtain the minimum value of  $\Delta n$  for guiding:

$$2n_2 \Delta n \left(\frac{2\pi}{\lambda_0}\right)^2 t^2 \geq \left(\frac{\pi}{2}\right)^2 \quad (2-43)$$

$$\Delta n \geq \frac{1}{32n_2} (\lambda_0/t)^2 \quad (2-44)$$

Operating at  $1.15\mu$ , a  $12\mu$  thick guide has a cutoff of  $.8 \times 10^{-4}$  for  $\Delta n$ . The next higher mode has a cutoff nine times higher; therefore, if  $\Delta n$  is properly chosen, the guide undergoes single mode ( $TE_1$  or  $TM_1$ ) operation.

The guide discussed above is related to a symmetric dielectric waveguide of twice the thickness  $2t$  and the same index discontinuity  $\Delta n = n_2 - n_3$ . The quantities  $ht$  and  $pt$  will be governed by the same equations 2-32 and 2-38 in addition to a new transcendental equation:

$$pt = ht \tan(ht) \quad (26) \quad (2-45)$$

The dashed lines in Figure IV starting from  $ht = 0, \pi,$  and  $2\pi$  correspond to its multiple solutions.

The intersection points of the dashed lines with the circles in Figure IV are the solutions for modes of even symmetry in a symmetric guide ( $TE_0, TE_2--$ ), and the other intersection points already mentioned are those for modes of odd symmetry ( $TE_1, TE_3--$ ):

$$\text{Even } |x| < t \quad E_y(x) \sim \cos(hx) \quad (2-46)$$

$$\text{Odd } |x| < t \quad E_y(x) \sim \sin(hx) \quad (2-47)$$

Figure V shows the mode profiles of the four lowest modes of a symmetric dielectric waveguide. The even modes have a field maximum and the odd modes have a zero point at the guide center. If, in the case of odd modes, we bisect the guide and look at the mode profile for  $0 < x < t$ , the remaining half is the same as the mode profile of the epitaxial waveguide discussed before. Thus, the epitaxial guide propagates the odd modes only of a symmetric guide of twice its thickness  $2t$  and same index discontinuity  $\Delta n = n_2 - n_3$ , and this to a very good approximation is independent of  $n_1$ , as long as  $|n_2^2 - n_1^2|$  is much larger than  $n_2^2 - n_3^2$ .

The longitudinal components  $H_z$  of the TE modes and  $E_z$  of the TM modes are very small. The curl equations give:

$$\text{TE} \quad H_z = \frac{i}{\omega\mu_0} \frac{\partial E_y}{\partial x} \quad (2-48)$$

$$\text{TE} \quad H_x = \frac{-i}{\omega\mu_0} \frac{\partial E_y}{\partial z} \quad (2-49)$$

$$\text{TM} \quad E_z = \frac{-i}{\omega n^2 \epsilon_0} \frac{\partial H_y}{\partial x} \quad (2-50)$$

$$\text{TM} \quad E_x = \frac{i}{\omega n^2 \epsilon_0} \frac{\partial H_y}{\partial z} \quad (2-51)$$

From 2-9 and 2-41, we have:

$$E_y, H_y \sim \sin(hx) \exp[i(\omega t - \beta z)] \quad 0 < x < t \quad (2-52)$$

Substituting 2-52 into 2-48, 2-49, 2-50, and 2-51, we obtain:

$$\text{TE} \quad |H_z| = \frac{h}{\beta} |H_x| \quad (2-53)$$

$$\text{TM} \quad |E_z| = \frac{h}{\beta} |E_x| \quad (2-54)$$

The guided mode propagation vector  $\beta$  is very close in magnitude to the plane wave propagation vector in a dielectric of the same refractive index  $n_2$  as the epitaxial guide. Omitting the small  $h^2$  term in equation 2-24, we have:

$$\beta \approx n_2 \left( \frac{2\pi}{\lambda_0} \right) \quad (2-55)$$

Let us consider a mode of the lowest order ( $\text{TE}_1$  or  $\text{TM}_1$ ) in the epitaxial guide. Equation 2-37 determines the range of  $ht$  for such a mode ( $m=0$ ). It is:

$$\frac{\pi}{2} < ht < \pi \quad (2-56)$$

From 2-55 and 2-56 we obtain:

$$\frac{\lambda_0}{4n_2 t} < \frac{h}{\beta} < \frac{\lambda_0}{2n_2 t} \quad (2-57)$$

Operating at  $1.15\mu$ , a  $12\mu$  thick guide gives the following range:

$$.7\% < \frac{h}{\beta} < 1.4\% \quad (2-58)$$

The longitudinal components are about 1% as large as the transverse ones and the modes are essentially TEM in character. Therefore, apart from the  $x$  dependence of the amplitude, the TE and TM modes behave like two orthogonal plane waves moving along  $z$  with TE fields  $E_y$  and  $H_x$  and TM fields  $E_x$  and  $H_y$ .

So far only the metal bounded waveguide has been considered. However, the analysis for guided modes in an air bounded guide is closely related to the analysis done up to this point for the metal bounded guide. Formally, the complex index  $n_1$  for the metal is replaced by  $n_1 = 1$  for air, and we start with the same equations 2-20, 2-26, 2-27, and 2-30 involving  $q$ ,  $h$ , and  $p$  for the TE and TM modes. For the metal bounded guide, these four relations were simplified and the modified results are 2-31, 2-32, and 2-38. The assumptions of  $n_2 - n_3 \ll 1$  and  $|n_2^2 - n_1^2| \gg n_2^2 - n_3^2$  were used to derive 2-31 and 2-32. To derive 2-38, the arguments  $q/h$  in 2-20 and  $(\frac{n_2}{n_1})^2 q/h$  in 2-30 were shown to be much larger in magnitude than one. All the same conditions also apply to the air bounded waveguide. Therefore, the three equations 2-31, 2-32, and 2-38 involving  $q$ ,  $h$ , and  $p$  are equally valid for both the air and metal bounded waveguides. These are the equations that lead to the ideal behavior of the TE and TM modes discussed before; namely that the fields approach zero at the air or metal interface and that the guide propagates the odd modes only of a symmetric dielectric waveguide of thickness  $2t$  and index discontinuity  $n_2 - n_3$ .

### 2.3 A Comparison of the Metal and Air Bounded Waveguides

The fields  $E_y(x)$  for the TE modes and  $H_y(x)$  for the TM modes, although very small, are not equal to zero at the air or metal-guide interface. The ratio of the field at the interface to the field maximum within the guide can be easily estimated. Referring to equations 2-39 and 2-40 which give  $E_y(x)$  and  $H_y(x)$ , we obtain:

$$\text{TE} \quad \frac{E_y(x=0)}{E_y(\text{Max})} = \frac{h}{q} \quad (2-59)$$

$$\text{TM} \quad \frac{H_y(x=0)}{H_y(\text{Max})} = \left(\frac{n_1}{n_2}\right)^2 \frac{h}{q} \quad (2-60)$$

For single mode ( $\text{TE}_1$  or  $\text{TM}_1$ ) propagation we have already set a range for  $h$ . From 2-56 we have:

$$\frac{\pi}{2t} < h < \frac{\pi}{t} \quad (2-61)$$

Substituting into 2-59 and 2-60, we obtain:

$$\text{TE} \quad \frac{\pi}{2tq} < \frac{E_y(x=0)}{E_y(\text{Max})} < \frac{\pi}{tq} \quad (2-62)$$

$$\text{TM} \quad \left(\frac{n_1}{n_2}\right)^2 \frac{\pi}{2tq} < \frac{H_y(x=0)}{H_y(\text{Max})} < \left(\frac{n_1}{n_2}\right)^2 \frac{\pi}{tq} \quad (2-63)$$

for single mode propagation. (We will not go into similar calculations for higher order modes since the guides used in the experimental work only propagated the lowest order  $\text{TE}_1$  or  $\text{TM}_1$  mode.)

Equation 2-31 gives  $q$ :

$$q \approx \sqrt{n_1^2 - n_2^2} \left(\frac{2\pi}{\lambda_0}\right) \quad (2-64)$$

Operating at  $1.15\mu$  in a  $12\mu$  thick guide we can now obtain magnitudes of the ratios of the field at  $x = 0$  to its maximum within the guide.

$$\text{Aluminum TE} \quad .2 \text{ to } 4\% \quad (2-65)$$

$$\text{Aluminum TM} \quad 2.0 \text{ to } 4.0\% \quad (2-66)$$

$$\text{Air TE} \quad .7 \text{ to } 1.4\% \quad (2-67)$$

$$\text{Air TM} \quad .06 \text{ to } .12\% \quad (2-68)$$

This confirms the original assumption of very small fields at the  $x = 0$  interface.

The fields at  $x = 0$  penetrate into the metal or air a small distance. The  $1/e$  depth for optical power is:

$$d = \frac{1}{2\text{Re}(q)} \quad (2-69)$$

This gives:

$$\text{Aluminum} \quad d = 90\text{\AA} \quad (2-70)$$

$$\text{Air} \quad d = 270\text{\AA} \quad (2-71)$$

The last aspect to be considered is the attenuation of the modes as they travel down the guide. There are small optical losses in the GaAs which have not been included in the model used so far; but the metal walled guide has additional metallic losses that should be considered. The very small imaginary parts of  $h$  and  $\beta$  which have been ignored so far are used to determine the attenuation of the modes.

The transcendental relations 2-20 and 2-30 express  $ht$  in terms of arc tangents with arguments in  $q/h$  and  $p/h$ . The imaginary

parts of  $h$  and  $p$  are assumed to be extremely small; however, the imaginary part of  $q$  is more sizable. From 2-33, it is about 15% the real part of  $q$ . It is this factor that will generate the imaginary part of  $ht$  in 2-20 and 2-30. The complex arguments in  $q$  for 2-20 and 2-30 are much larger than one in magnitude. Using this fact, the following approximations can be made for the lowest order modes:

$$TE_1 \quad ht \approx \tan^{-1}(p/h) + \frac{\pi}{2} - h/q \quad (2-72)$$

$$TM_1 \quad ht \approx \tan^{-1}(p/h) + \frac{\pi}{2} - \left(\frac{n_1}{n_2}\right)^2 h/q \quad (2-73)$$

this leads to:

$$TE_1 \quad ht \approx \left[ \tan^{-1}(p/h) + \frac{\pi}{2} \right] \left[ 1 - \frac{1}{qt} \right] \quad (2-74)$$

$$TM_1 \quad ht \approx \left[ \tan^{-1}(p/h) + \frac{\pi}{2} \right] \left[ 1 - \left(\frac{n_1}{n_2}\right)^2 \frac{1}{qt} \right] \quad (2-75)$$

$$0 < \tan^{-1}(p/h) < \pi/2 \quad (2-76)$$

Condition 2-76 gives the following range for the imaginary part of  $ht$ :

$$TE_1 \quad \frac{\pi}{2t} \operatorname{Im}\left(\frac{1}{q}\right) < \operatorname{Im}(ht) < \frac{\pi}{t} \operatorname{Im}\left(\frac{1}{q}\right) \quad (2-77)$$

$$TM_1 \quad \frac{\pi}{2t} \operatorname{Im}\left[\left(\frac{n_1}{n_2}\right)^2 \frac{1}{q}\right] < \operatorname{Im}(ht) < \frac{\pi}{t} \operatorname{Im}\left[\left(\frac{n_1}{n_2}\right)^2 \frac{1}{q}\right] \quad (2-78)$$

The propagation vector  $\beta$  has an imaginary part proportional to the imaginary part of  $h$ . Equation 2-24 gives the connection between  $\beta$  and  $h$ :

$$\beta \approx n_2 \left( \frac{2\pi}{\lambda_o} \right) \left[ 1 - \frac{1}{2n_2^2} \left( \frac{\lambda_o}{2\pi} \right)^2 h^2 \right] \quad (2-79)$$

$$\text{Im}(\beta) \approx \frac{\lambda_o}{4\pi n_2} \text{Im}(h^2) \quad (2-80)$$

Equation 2-80 can be further modified using the intermediate steps:

$$\text{Im}(h^2) \approx 2\text{Re}(h) \text{Im}(h) \quad (2-81)$$

$$\frac{\pi}{2t} < \text{Re}(h) < \frac{\pi}{t} \quad (2-82)$$

Equation 2-82 is the same as 2-61 in which  $h$  was taken as real. The range of the imaginary part of  $\beta$  is now set for the  $\text{TE}_1$  and  $\text{TM}_1$  modes:

$$\frac{\lambda_o}{4n_2 t} \text{Im}(h) < \text{Im}(\beta) < \frac{\lambda_o}{2n_2 t} \text{Im}(h) \quad (2-83)$$

Substitution of 2-77 and 2-78 into 2-83 gives:

$$\text{TE}_1 \quad \frac{\pi \lambda_o}{8n_2 t^3} \text{Im}\left(\frac{1}{q}\right) < \text{Im}(\beta) < \frac{\pi \lambda_o}{2n_2 t^3} \text{Im}\left(\frac{1}{q}\right) \quad (2-84)$$

$$\text{TM}_1 \quad \frac{\pi \lambda_o}{8n_2 t^3} \text{Im}\left[\left(\frac{n_1}{n_2}\right)^2 \frac{1}{q}\right] < \text{Im}(\beta) < \frac{\pi \lambda_o}{2n_2 t^3} \text{Im}\left[\left(\frac{n_1}{n_2}\right)^2 \frac{1}{q}\right] \quad (2-85)$$

Operating at  $1.15\mu$  in a  $12\mu$  thick guide, we put numbers into the equations for  $h$  and  $\beta$  and obtain:

$$1300 \text{ cm}^{-1} < \text{Re}(h) < 2600 \text{ cm}^{-1} \quad (2-86)$$

$$\text{TE}_1 \quad .26 \text{ cm}^{-1} < \text{Im}(h) < .53 \text{ cm}^{-1} \quad (2-87)$$

$$\text{TM}_1 \quad 2.5 \text{ cm}^{-1} < \text{Im}(h) < 5.0 \text{ cm}^{-1} \quad (2-88)$$

$$\text{TE}_1 \quad .0018 \text{ cm}^{-1} < \text{Im}(\beta) < .0073 \text{ cm}^{-1} \quad (2-89)$$

$$\text{TM}_1 \quad .017 \text{ cm}^{-1} < \text{Im}(\beta) < .070 \text{ cm}^{-1} \quad (2-90)$$

for single mode propagation. We see that the imaginary part of  $h$  is much less than one percent of the real part of  $h$  for both the  $\text{TE}_1$  and  $\text{TM}_1$  modes. The  $1/e$  attenuation distance for mode power in the guide is:

$$d = \frac{1}{2\text{Im}(\beta)} \quad (2-91)$$

Putting in numbers, we have:

$$\text{TE}_1 \quad 68 \text{ cm} < d < 280 \text{ cm} \quad (2-92)$$

$$\text{TM}_1 \quad 7.1 \text{ cm} < d < 29 \text{ cm} \quad (2-93)$$

The losses in the metal are so small that we obtain attenuation distances tens of centimeters long. These losses are much smaller than the losses in the GaAs guide itself which give an attenuation distance on the order of one centimeter.

In short, even after considering all the additional factors, the  $\text{TE}_1$  and  $\text{TM}_1$  modes of both the air and metal walled guides are essentially the same.

## Chapter 3

### Metal-Semiconductor Junction

#### 3.1 Surface States

Due to a termination of the crystal lattice, localized surface states having energies distributed in the forbidden gap exist at the free surface of a semiconductor.<sup>(27)</sup> When there is no net charge on the surface atoms, these surface states are partially filled with electrons. In n-type material, if the surface states density is high enough, conduction band electrons move from a region adjacent to the surface into the surface states. This generates a double layer consisting of a positive space charge region and a negative surface charge layer.<sup>(27)</sup>

A surface states density exceeding about  $10^{13} \text{ cm}^{-2}$  has a surface Fermi level fixed at a definite position with respect to the conduction band edge that is independent of the interior Fermi level. This arises from the fact that the surface states density is so high that sizable transfers of charge in and out of the surface states scarcely move the surface Fermi level at all. The same insensitivity of the surface Fermi level occurs when a metal is deposited on the surface. The difference in work functions between metal and semiconductor is compensated by electrons moving from the semiconductor surface states into the metal, and the metal's Fermi level is locked at the free surface Fermi level. The level is independent to within two-tenths of a volt of the metal used, the semiconductor doping, the junction biasing voltage, the crystal orientation, or the existence of

an oxide monolayer in the junction. (28)

GaAs falls into a large class of surface states dominated semiconductors that observe the two-thirds rule. (29)

$$E_C - E_F = \frac{2}{3} E_G \quad (3-1)$$

The surface states fix the metal's Fermi level about two-thirds of the band gap energy below the conduction band edge. For aluminum on GaAs:

$$E_C - E_F = .80 \text{ eV} \quad (3-2)$$

This quantity is  $e\phi_B$ , the barrier potential of the Schottky barrier discussed in the next section.

### 3.2 Schottky Barrier

Figure VI depicts the Schottky barrier with no applied voltage in which the energy bands are bent upward near the junction to keep the Fermi level constant everywhere under thermal equilibrium. For aluminum on n-type GaAs, the upturned bands produce a barrier potential of .80 eV that electrons in the metal must climb to reach the semiconductor, and a diffusion potential of .64 eV that conduction electrons in the semiconductor must climb to reach the metal. The donor levels, which lie about .002 eV below the conduction band, are ionized, giving up their electrons to the conduction band. Near the junction where the bands are upturned, by increasing the electron energy, the conduction electrons are swept out yielding a positive space charge region of depletion layer width  $w$ . There must be a negative surface layer too.

The application of a negative voltage to the aluminum increases the electron energy and hence the Fermi level of the metal with respect to the semiconductor energy bands. This is the reverse bias condition used for modulation purposes shown in Figure VII. Here is shown the energy band structure along with the electric field and space charge in the depletion region that grows in size as the reverse biasing voltage is increased. With no applied voltage, the width  $w$  of the space charge region is determined by the built in or diffusion voltage. Assuming a constant donor density  $N_D$ , the diffusion voltage and the maximum electric field at  $x = 0$  can be determined.

$$V_D = \frac{N_D e}{2\epsilon} w^2 \quad (3-3)$$

$$E(x = 0) = \frac{2}{w} V_D \quad (3-4)$$

For the barrier used in our work:

$$\epsilon = 11\epsilon_0 \quad (3-5)$$

$$N_D = 10^{15} \text{ cm}^{-3} \quad (3-6)$$

$$V_D = .64 \text{ v} \quad (3-7)$$

$$w = .9\mu \quad (3-8)$$

$$E(x = 0) = 1.5 \times 10^4 \text{ v/cm} \quad (3-9)$$

The above is derived for a space charge region with a sharp edge at  $w$ . If the conduction electron distribution around  $w$  is included, a

4% correction to  $V_D$  of  $-kT/e$  has to be made. (30)

Applying a reverse biasing voltage increases the width and maximum electric field of the depletion layer.

$$V_A + V_D = \frac{N_D e}{2} w^2 \quad (3-10)$$

$$E(x = 0) = \frac{2}{w}(V_A + V_D) \quad (3-11)$$

For  $V_A = 100$  v:

$$w = 11\mu \quad (3-12)$$

$$E(x = 0) = 1.8 \times 10^5 \text{ v/cm} \quad (3-13)$$

The width and the field have gone up by a factor of twelve from the zero voltage biasing case.

The refractive index is changed by the field through the electrooptic effect. The maximum change in the space charge layer is:

$$\Delta n_{Eo} = \pm \frac{1}{2} n_o^3 r_{41} E(x = 0) \quad (3-14)$$

This result is derived from equation 1-25 in section 1.3. For  $V_A = 100$ v we have:

$$\Delta n_{Eo} = \pm 4.8 \times 10^{-4} \quad (3-15)$$

The index variation with  $x$  is proportional to the electric field variation as shown in Figure VII, with the maximum index change at the junction ( $x = 0$ ).

### 3.3 Barrier Capacitance

The Schottky barrier space charge region is examined by measuring its AC differential capacitance as a function of applied voltage. Depletion layer width  $w$  at voltage  $V_A$  is increased to  $w + dw$  by voltage increment  $dV$ . (31)

$$C = \left. \frac{dQ}{dV} \right|_{V_A} \quad (3-16)$$

$$C = \frac{\epsilon A}{w} \quad (3-17)$$

$$dQ = eN_D A dw \quad (3-18)$$

$N_D(w)$  is the free carrier density at the edge of the depletion region, and it is assumed to be equal to the donor density. Eliminating  $w$  we obtain:

$$N_D(w) = \frac{2}{\epsilon e A^2} \left. \frac{dV}{d[1/c^2]} \right|_{V_A} \quad (3-19)$$

Figure VIII shows a representative plot of  $V_A$  as a function of  $\frac{1}{c^2}$  for a Schottky barrier made on one of the light modulators. The slope is proportional to  $N_D(w)$  according to 3-19, and the straight dotted line represents an average value of  $N_D$  for the barrier. Derived from this graph is a plot of  $N_D(w)$  as a function of  $w$  shown in Figure IX.  $N_D$  is by no means the constant  $10^{15} \text{ cm}^{-3}$  used for calculations in the last section.

$$\begin{array}{ll} V_A = 0_V & V_A = 140v \\ w = 2.7\mu & w = 12.2\mu \\ N_D = .4 \times 10^{15} \text{ cm}^{-3} & N_D = 1.7 \times 10^{15} \text{ cm}^{-3} \end{array} \quad (3-20)$$

The extrapolated dotted line in Figure IX extends beyond the breakdown voltage of about 140 volts into the substrate where  $N_D$  is over  $20 \times 10^{15} \text{ cm}^{-3}$ . Only in a few of the barriers made was punch-through into the substrate observed; most junctions broke down before this point at lower voltages.

At the other end of the scale for  $V_A = 0v$ , the built-in barrier width is  $2.7\mu$ . Putting into equation 3-3 a diffusion voltage of  $.6v$  and a width of  $2.7\mu$ , we obtain an average  $N_D$  of about  $.1 \times 10^{15} \text{ cm}^{-3}$  inside the built-in barrier. This  $N_D$  is considerably less than the  $.4 \times 10^{15} \text{ cm}^{-3}$  measured at the barrier edge. Possibly, the combination of a thin insulating layer between metal and semiconductor and a built-in barrier with an  $N_D$  between  $.1$  and  $.4 \times 10^{15} \text{ cm}^{-3}$  gives a width of  $2.7\mu$ . Most of the large Schottky barriers had even wider barrier widths for  $V_A = 0$ . This sort of behavior is not well understood, but is of minor importance in studying the waveguided light.

### 3.4 Barrier Current

Another indicator of the Schottky barrier is the diode characteristic of current as a function of voltage. The following equations give the ideal behavior observed in Schottky barriers with areas less than  $10^{-2} \text{ mm}^2$  consisting of Gold deposited on n-type GaAs. (30,32)

$$I = I_S \left[ \exp\left(\frac{eV}{kT}\right) - 1 \right] \quad (3-21)$$

$$I_S = A_R T^2 \exp\left(-\frac{e\phi_B}{kT}\right) \quad (3-22)$$

$$A_R \sim 200 - 600 \text{ mA/mm}^2 \text{ } ^\circ\text{k}^2 \quad (3-23)$$

Aluminum on n-type GaAs is assumed to give similar numbers for  $A_R$ .

The reverse biasing voltage of the last section  $V_A = -V$ ; and  $e\phi_B$ , the barrier potential is .80 eV for aluminum. We have the following:

Reverse bias:

$$eV \ll -kT \quad T = 300^\circ\text{k} \quad (3-24)$$

$$I = -I_S \\ \sim -10^{-6} \text{ mA/mm}^2 \quad (3-25)$$

Forward bias:

$$eV \gg kT \quad T = 300^\circ\text{k} \quad (3-26)$$

$$I = I_S \exp\left(\frac{eV}{kT}\right) \\ \sim 10^{-2} \text{ mA/mm}^2 \quad \text{at } V = .25\text{v} \quad (3-27)$$

The Schottky barriers made for the modulator have areas greater than  $1 \text{ mm}^2$ , and did not conform to ideal behavior obtained with the barriers with areas less than  $10^{-2} \text{ mm}^2$ . In the reverse direction, high voltages yielded leakage currents thousands of times the ideal of  $10^{-6} \text{ mA/mm}^2$ , and in the forward direction, the turn over point around  $10^{-2} \text{ mA/mm}^2$  was reached at about one volt instead of the ideal of .25v. Thus, the diode current behavior of the modulator Schottky barriers was a much

rougher approximation to the ideal than the capacitance data, and was only used as an indicator of the reverse biasing voltage breakdown point.

Electrooptic Waveguide Modulator

4.1 Index Profile

In Chapter 2 we examined the guided wave solutions in a passive epitaxial thin film structure. The thin film had a constant index  $n_2$  as shown in Figure III, and guiding could occur because the thin film index  $n_2$  was greater than the substrate index  $n_3$ .

In this chapter we will apply a modulation voltage to the guide and perturb these results. The modified index profile is shown in Figure X. Application of a reverse biasing voltage to the aluminum electrode generates a space charge region in the thin film for  $0 < x < w$ . This in turn produces a DC electric field that increases from zero at  $x = w$  to a maximum at  $x = 0$ .

The aluminum is evaporated on the (100) plane and light travels either in the  $z = [011]$  or the perpendicular  $z = [10\bar{1}]$  direction. Following the electrooptic modulator equations 1-20 through 1-22 we see that a modulating field  $E_{DC}$  along  $x$  creates a positive or negative change in index  $\Delta n_{EO}$  in the depletion region  $0 < x < w$  for TE light polarized perpendicular to  $x$ , and no change in index for TM light polarized parallel to  $x$ . For TE light,  $\Delta n_{EO}$  is opposite and equal for the two possible directions of propagation  $z = [011]$  and  $z = [01\bar{1}]$ . If  $\Delta n_{EO}$  is positive for one of the beam directions in the crystal, rotation of the crystal by  $90^\circ$  about the  $x$  axis makes  $\Delta n_{EO}$  negative.

If we assume a constant doping level  $N_D$  in the guide film, we have:

$$\Delta n_{EO}(x) = \pm \Delta n_{EO} \left( \frac{w-x}{w} \right) \quad (4-1)$$

in which

$$\Delta n_{EO} = \frac{1}{2} n_2^3 r_{41} E(x = 0) \quad (4-2)$$

from equation 3 - 14 and

$$E(x = 0) = \frac{2}{w} (V_A + V_D) \quad (4-3)$$

from equation 3 - 11.

The linearity of  $\Delta n_{EO}(x)$  with respect to  $x$  is shown in Figure X for both polarities. As determined from the capacitance data, the actual epitaxial layers used generally had  $N_D(x)$  increase with  $x$ , giving a solution to  $\Delta n_{EO}$  that is flatter than the linear approximation near  $x = 0$  and steeper near  $x = w$ . In addition, with no external modulating field, we still have a small residual  $\Delta n_{EO}$  from the built in voltage  $V_D$  that we can safely ignore in the guided wave calculations of the following sections.

#### 4.2 Guided Wave Solutions

When the DC modulating field is turned on, the index profile of Figure X no longer has constant index regions everywhere all giving mode solutions in term of real and imaginary exponentials. The index profile now has four regions.

$$x < 0 \quad n_1 \quad \text{complex} \quad (4-4)$$

$$0 < x < w \quad n_2 \pm \Delta n_{EO} \left[ \frac{w-x}{w} \right] \quad (4-5)$$

$$w < x < t \quad n_2 \quad (4-6)$$

$$x > t \quad n_3 \quad (4-7)$$

The mode fields at  $x = 0$  are very small. For the passive waveguide with no external modulation field, they were shown to be 4% (Equation 2-66) or less of the mode maximum within the guide. To make headway in this more complicated case, we set them equal to zero. We have also assumed that doping density  $N_D$  is a constant, giving an index that is a linear function of  $x$  in the depletion layer  $0 < x < w$ . The optical fields for the TE modes are:

$$\text{Region 1} \quad 0 < x < w \quad E_y(x) = E_1(x) \quad (4-8)$$

$$\text{Region 2} \quad w < x < t \quad E_y(x) = B \exp(ihx) + C \exp(-ihx) \quad (4-9)$$

$$\text{Region 3} \quad x > t \quad E_y(x) = D \exp[-p(x-t)] \quad (4-10)$$

Regions 2 and 3 have constant values  $n_2$  and  $n_3$  for the refractive index; so the solutions to  $E_y(x)$  are unchanged. The solution  $E_1(x)$  in the space charge region 1 is more complicated. The assumed index variation in  $0 < x < w$  is:

$$n = n_2 \pm \Delta n_{EO} \left( \frac{w-x}{w} \right) \quad (4-11)$$

with the boundary condition

$$E_1(x = 0) = 0 \quad (4-12)$$

The wave equation  $\nabla^2 E_1 + k_1^2(x)E_1 = 0$  becomes

$$\frac{d^2 E_1}{dx^2} + \left[ n_2^2 \left( \frac{2\pi}{\lambda_0} \right)^2 - \beta^2 \right] E_1 \quad (4-13)$$

$$\pm 2 n_2 \Delta n_{EO} \left( \frac{2\pi}{\lambda_0} \right)^2 \left( \frac{w-x}{w} \right) E_1 = 0$$

The first two terms of 4-13 give the wave equation for a constant index region  $n_2$  ; this part is the same as equation 2-21. The last term is a perturbation on the first part due to the electrooptic modification of the index  $\Delta n_{EO} \left( \frac{w-x}{w} \right)$  . Using equation 2-24, we can rewrite 4-13:

$$\frac{d^2 E_1}{dx^2} + h^2 E_1 \pm \Delta \left[ \frac{w-x}{w} \right] E_1 = 0 \quad (4-14)$$

where

$$\Delta = 2 n_2 \Delta n_{EO} \left( \frac{2\pi}{\lambda_0} \right)^2 \text{ from equation 4-13.} \quad (4-15)$$

Condition 4-12 and Equation 4-14 are solved by a linear combination of Airy functions of the first and second kind,  $Ai(-z)$  and  $Bi(-z)$ .<sup>(33)</sup> Writing down  $E_1(x)$  for region 1 for  $0 < x < w$  , we have:

$$\begin{aligned} E_1(x) &= E_1(z) \\ &= A \left[ Bi[-z(0)]Ai(-z) - Ai[-z(0)]Bi(-z) \right] . \end{aligned} \quad (4-16)$$

The argument  $z$  is a function of  $x$  .

$$z = \left( \frac{w}{\Delta} \right)^{2/3} \left[ h^2 \pm \Delta \left( \frac{w-x}{w} \right) \right] \quad (4-17)$$

and

$$\begin{aligned} z(0) &= z(x = 0) \\ &= \left(\frac{w}{\Delta}\right)^{2/3} [h^2 \pm \Delta] \end{aligned} \quad (4-18)$$

At  $x = w$  and  $x = t$ ,  $E_y$  and  $\frac{\partial E_y}{\partial x}$  are continuous. In a fashion similar to what was done at  $x = 0$  and  $x = t$  for the passive waveguide, we write down four equations similar to (2-13), (2-14), (2-17), and (2-18) that can be solved by setting up a four by four determinant that must equal zero to give non-zero A, B, C, and D coefficients. Solving the determinant, we obtain:

$$\frac{1}{E_1} \left. \frac{dE_1}{dz} \right|_{z(w)} = \pm h \left(\frac{w}{\Delta}\right)^{1/3} \frac{h \tan [h(t-w)] - p}{p \tan [h(t-w)] + h} \quad (4-19)$$

At cut off,  $p$  goes to zero. This simplifies (4-19).

$$\frac{1}{E_1} \left. \frac{dE_1}{dz} \right|_{z(w)} = \pm h \left(\frac{w}{\Delta}\right)^{1/3} \tan [h(t-w)] \quad (4-20)$$

Substitution of (4-16) into (4-20) gives:

$$\begin{aligned} &\frac{Bi[-z(0)]Ai'[-z(w)] - Ai[-z(0)]Bi'[-z(w)]}{Bi[-z(0)]Ai[-z(w)] - Ai[-z(0)]Bi[-z(w)]} \\ &= \pm h \left(\frac{w}{\Delta}\right)^{1/3} \tan[h(t-w)] \end{aligned} \quad (4-21)$$

where

$$h \left(\frac{w}{\Delta}\right)^{1/3} = [z(w)]^{1/2} \quad (4-22)$$

from equation (4-17) and

$$z(0) = z(w) \left[ 1 \pm \frac{\Delta}{h^2} \right] \quad (4-23)$$

from (4-18) and (4-22).

Cut off condition (4-21) is dependent on the four terms  $\Delta$ ,  $w$ ,  $h$ , and  $t$ .  $t$  is just the thickness of the epitaxial layer, and  $w$  is the width of the space charge region with the assumption that  $w < t$ .  $\Delta$  is proportional to  $w$ . Substitution of (4-2), (4-3), and (3-10) into (4-15) yields:

$$\Delta = \left[ n_2^4 r_{41} \frac{N_D e}{\epsilon} \left( \frac{2\pi}{\lambda_0} \right)^2 \right] w \quad (4-24)$$

The factors in brackets are all constants. The remaining term  $h$  is given by equation (2-23) with  $p = 0$  because we are operating at cutoff.

$$h = \frac{2\pi}{\lambda_0} \sqrt{2n_2 \Delta n} \quad (4-25)$$

We see that  $h$  depends on the built in index difference  $\Delta n = n_2 - n_3$ . Using a fixed value of  $\Delta n$ , we can determine the electrooptic perturbation  $\Delta n_{EO}$  necessary for attaining waveguide cutoff.  $\Delta n_{EO}$  is proportional to  $w$ . Substitution of (4-3) and (3-10) into (4-2) gives:

$$\Delta n_{EO} = \left[ \frac{1}{2} n_2^3 r_{41} \frac{N_D e}{\epsilon} \right] w \quad (4-26)$$

With  $t$ ,  $\Delta n$ , and  $h$  fixed, the only independent variable remaining is  $w$ . Numerically, we find the right value of  $w$  to solve equation (4-21). From (4-26) we then obtain the value of  $\Delta n_{EO}$  for attaining waveguide cutoff.

### 4.3 Electrooptic Switching

Equation (4-21) gives the cutoff condition for the lowest order  $TE_1$  mode in the electrooptic modulator. Changing the index about this point can switch the guide from a non-guiding to a guiding state. The + sign in (4-21) corresponds to the case in which an external modulating field increases the index in the space charge region above  $n_2$ . If the epitaxial film with field off is below wave guide cut off, turning the field on can increase  $n_2$ , sending the guide through the cut off point determined by (4-21).

The same arguments apply in the opposite sense for the - sign case. The doping profile in Figure IX depicts an epitaxial film with an average  $N_D$  of about  $1.0 \times 10^{15} \text{ cm}^{-3}$  and a thickness around  $12.5\mu$ . With the DC modulating field off, the substrate has to be sufficiently doped to generate through free carrier depression of the index, a big enough index difference between guiding film and substrate to permit wave guiding to occur. Operating at  $1.15\mu$ , equation (2-44) gives the index difference  $\Delta n = n_2 - n_3$  for wave guide cut off.

$$\Delta n = .77 \times 10^{-4} \quad (4-27)$$

The difference in doping between substrate and guiding film is proportional to  $\Delta n$ . From equation (1-10) we have:

$$\begin{aligned} N_D (\text{substrate}) - N_D (\text{epilayer}) \\ = 4.2 \times 10^{20} \Delta n \end{aligned} \quad (4-28)$$

at cut off,  $\Delta n = .77 \times 10^{-4}$ , which gives:

$$N_D \text{ (substrate)} = 3.1 \times 10^{16} \text{ cm}^{-3} \quad (4-29)$$

assuming that  $N_D \text{ (epilayer)} = 1 \times 10^{15} \text{ cm}^{-3}$ . This is the amount of substrate doping necessary to attain waveguide cut off in a  $12.5\mu$  guide with the modulating field off. Increased doping enhances waveguiding; decreased doping wipes it out.

If  $N_D \text{ (substrate)}$  in a  $12.5\mu$  guide has a value different from the one given in (4-29), the index has to be modified electrooptically to attain cutoff. For a given  $N_D \text{ (substrate)}$  and  $N_D \text{ (epilayer)}$ , we have a value of  $\Delta n$  given by (4-28). Using this value of  $\Delta n$ , we find the correct value of the depletion layer width  $w$  to solve cutoff equation (4-21). Knowing  $w$ , we can easily determine the maximum modulation cutoff voltage  $V_{CO}$ , the maximum index shift  $\Delta n_{EO}$  to accomplish optical switching, and the maximum modulation field  $E(x=0)$ .

Let us consider two cases for electrooptic switching of the  $TE_1$  mode in a  $12.5\mu$  guide with  $N_D \text{ (epilayer)} = 1 \times 10^{15} \text{ cm}^{-3}$ . In the first, substrate doping is 50% above the threshold in (4-29), and waveguiding is wiped out by decreasing the index electrooptically. This gives us:

$$N_D \text{ (substrate)} = 4.6 \times 10^{16} \text{ cm}^{-3} \quad (4-30)$$

$$\Delta n = 1.15 \times 10^{-4} \quad (4-31)$$

By means of cutoff equation (4-21), we obtain:

$$w = 8.5\mu \quad (4-32)$$

From (3-11), (4-2), (4-3), and (4-26), we have:

$$E (x=0) = \frac{N_D e}{\epsilon} w \quad (4-33)$$

$$V_{co} = \frac{N_D e}{2\epsilon} w^2 \quad (4-34)$$

$$\Delta n_{EO} = \left[ \frac{1}{2} n_2^3 r_{41} \frac{N_D e}{\epsilon} \right] w \quad (4-35)$$

Substitution of (4-32) into (4-33), (4-34), and (4-35), gives:

$$E (x=0) = 1.4 \times 10^5 \text{ v/cm} \quad (4-36)$$

$$V_{co} = 60 \text{ v} \quad (4-37)$$

$$\Delta n_{EO} = 3.7 \times 10^{-4} \quad (4-38)$$

In the second case, substrate doping is 50% below the threshold value in 4-29, and waveguiding is generated by increasing the index.

We have:

$$N_D (\text{substrate}) = 1.5 \times 10^{16} \text{ cm}^{-3} \quad (4-39)$$

$$\Delta n = .38 \times 10^{-4} \quad (4-40)$$

Cutoff equation 4-21 gives:

$$w = 8.0 \mu \quad (4-41)$$

From (4-33), (4-34), and (4-35), we obtain:

$$E(x = 0) = 1.3 \times 10^5 \text{ v/cm} \quad (4-42)$$

$$V_{CO} = 52\text{v} \quad (4-43)$$

$$\Delta n_{EO} = 3.4 \times 10^{-4} \quad (4-44)$$

Figure XI shows the index profiles for cases 1 and 2 in contrast to case 3, the built in index profile for waveguide cutoff at  $V = 0$ . The maximum electrooptic index shift  $\Delta n_{EO}$  is much larger than the built in index difference  $\Delta n = n_2 - n_3$ . For cases 1 and 2, if a constant average field acts to raise or lower the index uniformly across the entire  $12.5\mu$  layer, it would have to give an index shift of 50% the built in difference of case 3 for the guide to reach cut off.

$$\begin{aligned} \Delta n_{EO} \text{ (average)} &= \frac{1}{2} (n_2 - n_3) \\ &= .38 \times 10^{-4} \end{aligned} \quad (4-45)$$

$$\Delta n_{EO} \text{ (average)} = \frac{1}{2} r_{41} n_2^3 E \text{ (average)} \quad (4-46)$$

$$E \text{ (average)} = 1.5 \times 10^4 \text{ v/cm} \quad (4-47)$$

The average field and average electrooptic index shift to attain cutoff are about 10% of the maximums for case 1 and case 2 in Figure XI. The space charge and electric field distributions in the epitaxial film are

shown in Figure XII. The top half corresponds to no punch through in which the space charge region does not penetrate into the substrate. This is the situation for the index profile just considered in Figure XI. The bottom half corresponds to punch through in which the space charge region penetrates into the substrate. The penetration into the substrate is very small because the substrate doping is much higher than the epitaxial layer doping.

In the limit of strong punch through, the electric field in the guide film is essentially constant and equal to  $V/t$  where  $V$  is the applied voltage:

$$0 < x < t \quad E = \frac{V}{t} \quad (4-48)$$

$$0 < x < t \quad \Delta n_{EO} = \frac{1}{2} r_{41} n_2^3 \frac{V}{t} \quad (4-49)$$

Here,  $\Delta n_{EO}$  is a constant across the entire guide region.

Below the limit of strong punch through,  $\Delta n_{EO}$  is variable across the guide and an equivalent average  $\Delta n_{EO}$  along the lines of (4-46) can be used.

$$\Delta n_{EO} \text{ (average)} = \frac{\eta}{2} r_{41} n_2^3 \frac{V}{t} \quad (4-50)$$

$\eta$  is an adjustable parameter with a maximum value of one for the case of strong punch through. For the electrooptic switching through cutoff shown in Figure XI,  $\eta$  is about 30%.

#### 4.4 Physical Significance of Cutoff

In Figure XIII, four  $TE_1(TM_1)$  intensity profiles are depicted for four different values of  $\Delta n = n_2 - n_3$  in a passive guide of thickness  $t$ .

$$x < t \tag{4-51}$$

$$I(x) \sim \sin^2(hx)$$

$$x > t \tag{4-52}$$

$$I(x) \sim \exp [-2p(x - t)]$$

At the cut off point  $\Delta n = \Delta n_{co}$ ,  $p = 0$  and the exponential tail extends an infinite distance into the substrate; and a vanishingly small percentage of the guided energy is contained in the epitaxial layer.

As  $\Delta n$  is increased, the mode energy becomes more concentrated and the peak of the intensity profile shifts to lower values of  $x$ . Table I gives the full width at half maximum and the position  $x_p$  of the peak intensity for each of the distributions in Figure XIII.

Table I

$\Delta n$	$x_p$	Full Width at Half Maximum (FWHM)
$1.5 \Delta n_{co}$	.85t	1.16t
$2 \Delta n_{co}$	.77t	.86t
$4 \Delta n_{co}$	.67t	.68t

In the limit of very large  $\Delta n$ , both  $x_p$  and FWHM approach  $.50t$ .

A modulation voltage introduces a triangular bump starting from  $x = 0$  in the index profile of Figure XIII for the  $TE_1$  mode. For a positive bump of maximum height  $\Delta n_{EO}$ , the intensity profile moves to the left; for a negative bump the profile moves to the right.

#### 4.5 Intensity Modulation

Electrooptic switching operates with the  $TE_1$  mode only, and with the built in index difference  $n_2 - n_3$  due to substrate doping near cutoff. At higher substrate doping levels,  $n_2 - n_3$  increases to the extent that modulation fields do not depress the guide index nearly enough to achieve cutoff, and the guide can no longer be used as an optical switch.

When the guide is used as an electrooptic intensity modulator, light is coupled into the guide with equal  $TM(E_x)$  and  $TE(E_y)$  components. With no modulation field, and operating below cutoff for the higher order modes, there is no electrooptic phase shift of the  $TE_1$  mode with respect to the  $TM_1$  mode in a guide of length  $L$ .

$$\begin{aligned} V = 0 \quad \Gamma &= [\beta_{TE} - \beta_{TM}] L \\ &= 0 \end{aligned} \tag{4-53}$$

When the modulation field is turned on the  $TE_1$  mode is phase shifted with respect to the unaffected  $TM_1$  mode.

$$\begin{aligned} V \neq 0 \quad \Gamma &= [\beta_{TE} - \beta_{TM}] L \\ &= \frac{2\pi L}{\lambda_0} \Delta n_{EO} \end{aligned} \tag{4-54}$$

where

$$\Delta n_{EO} = \frac{\bar{n}}{2} r_{41} n_2^3 \frac{V}{t} \quad (4-55)$$

This  $\Delta n_{EO}$  is the same as the average  $\Delta n_{EO}$  in (4-50).

In the standard intensity modulation experiment, light enters the guide at  $z = 0$  after being sent through a polarizer aligned at  $45^\circ$  midway between the  $+x$  and  $+y$  axes. After propagating down the guide, the light exits from the guide at  $z = L$ , and part of it is transmitted through an analyzer aligned at  $-45^\circ$  (i.e. crossed with respect to the input polarizer). For the special case of no modulation voltage, the index profiles for both the TE and TM polarized light are the same and the guided light is evenly divided between the  $TE_1$  and  $TM_1$  modes.

$$|E_y| = |E_x| \quad (4-56)$$

With the modulation voltage on, the  $TE_1$  index profile changes and (4-56) is no longer true. For a built in index difference  $\Delta n$  a few times above cut off, an electrooptic index shift  $\Delta n_{EO}$  can alter the shape and overall amplitude of the  $TE_1$  mode. Effects of this nature are shown in Figure XIII where the intensity or amplitude squared of the  $TE_1$  profile is changed.

Application of a modulation voltage gives us:

$$TE_1 \quad E_y = E_y(x) e^{-i\beta_{TE}z} \quad (4-57)$$

$$TM_1 \quad E_x = E_x(x) e^{-i\beta_{TM}z} \quad (4-58)$$

$E_y(x)$  and  $E_x(x)$  remain constant as the modes propagate down the guide in the  $z$  direction, whereas the phase between the modes is continually changing. The modes are in phase at  $z = 0$  where light enters the guide; they are phase shifted at  $z = L$  where light leaves the guide.

$$z = 0 \tag{4-59}$$

$$\frac{E_y}{E_x} = \frac{E_y(x)}{E_x(x)}$$

$$z = L \tag{4-60}$$

$$\frac{E_y}{E_x} = \frac{E_y(x)}{E_x(x)} \exp[i\Gamma]$$

The phase shift  $\Gamma$  has already been evaluated in (4-54).

To calculate the intensity of the output light that the analyzer transmits, the guided field amplitude as a function of  $x$  must first be determined at  $z = L$ .

$$\vec{E}(x) = \hat{x} E_x(x) + \hat{y} E_y(x) e^{i\Gamma} \tag{4-61}$$

$$I(x) = \vec{E}(x) \cdot \vec{E}(x)^* \tag{4-62}$$

$$= E_x(x)^2 + E_y(x)^2$$

$$I = \int_0^\infty I(x) dx \tag{4-63}$$

$$= I_{xx} + I_{yy}$$

I is the total guided light intensity incident on the analyzer, and is the sum of  $I_{xx}$ , the  $TM_1$  light intensity and  $I_{yy}$ , the  $TE_1$  light intensity.

The analyzer only transmits that component of  $\vec{E}(x)$  in (4-61) parallel to its polarization axis set at  $-45^\circ$ .

$$\begin{aligned} E_{\parallel}(x) &= \vec{E}(x) \cdot \frac{\hat{x} - \hat{y}}{\sqrt{2}} \\ &= \frac{1}{\sqrt{2}} [E_x(x) - E_y(x) e^{i\Gamma}] \end{aligned} \quad (4-64)$$

$$\begin{aligned} I_{\parallel}(x) &= E_{\parallel}(x) E_{\parallel}(x)^* \\ &= \frac{1}{2} [E_x(x)^2 + E_y(x)^2 - 2 E_x(x) E_y(x) \cos \Gamma] \end{aligned} \quad (4-65)$$

$$\begin{aligned} I_{\parallel} &= \int_0^{\infty} I_{\parallel}(x) dx \\ &= \frac{1}{2} [I_{xx} + I_{yy} - 2 I_{xy} \cos \Gamma] \end{aligned} \quad (4-66)$$

$I_{\parallel}$  is the total guided light intensity transmitted by the analyzer. For the special case in which the electrooptic index shift  $\Delta n_{EO}$  is very much smaller than the built in index discontinuity  $\Delta n = n_2 - n_3$  between the epitaxial layer and substrate, equation (4-56) is a good approximation. Then we have:

$$I_{xx} = I_{yy} = I_{yx} = \frac{I_o}{2} \quad (4-67)$$

and

$$I_{||} = I_o \sin^2 \frac{\Gamma}{2} \quad (4-68)$$

The output light intensity expressed in (4-66) contains three quantities dependent on the modulation voltage:  $I_{yy}$ , the  $TE_1$  light intensity;  $I_{xy}$ , the integrated product of the  $TE_1$  and  $TM_1$  mode amplitudes; and  $\Gamma$ , the relative phase shift.

$I_{yy}$  goes up or down depending on whether the  $TE_1$  index profile is raised or lowered by the modulation voltage. The behavior of  $I_{xy}$  is similar, although there is the additional factor of overlap between the  $TE_1$  and  $TM_1$  amplitude profiles to be considered as the  $TE_1$  profile is changed by applying a voltage. The relative phase shift  $\Gamma$  is a function of a number of factors. From (4-54) and (4-55):

$$\Gamma = \pi r_{41} n_2^3 \frac{\eta V L}{\lambda_o t} \quad (4-69)$$

For a given modulator, it appears that  $\Gamma$  is proportional to  $V$ , the applied voltage. However, the parameter  $\eta$  is not a constant over a wide voltage range. Below the limit of strong punch through, increasing the voltage extends the space charge region so that the refractive index is modulated in a larger percentage of the total guiding region leading to more efficient modulation. In other words, doubling the

modulation voltage more than doubles the phase shift  $\Gamma$  . This discussion is analogous to the discussion on  $\Delta n_{EO}$  that led to equation (4-50) in section 4.3.

One additional point is a built in birefringence from effects like strain that can shift  $\Gamma$  in (4-53) from a zero point at  $V = 0$  . The shift can be many times the built in Schottky barrier voltage of .6v which has been ignored in the above treatment.

Chapter 5

The Experiments

5.1 Sample Preparation

The GaAs samples were obtained from the United Aircraft Research Laboratories and from Monsanto in the form of flat pieces about one-half square inch in area and 25 mils thick. They consisted of 9-13 $\mu$  thick epitaxial layers deposited on (100) substrates. The electron mobility is about 6000 cm<sup>2</sup>/Vsec, giving resistivities of about 1 ohm cm in the epitaxial layers and from .01 to .1 ohm cm in the substrates.

From each piece several dozen individual waveguide modulators can be fabricated. First it is uniformly polished down on the substrate side. This is done by fixing the sample in wax, epitaxial side down, on a glass disc which is placed in a rotating beaker containing sulfuric acid-peroxide etch. The sample is then polished in the etch by another glass disc rubbing against it. The final thickness is nine mils or less. This thickness is suitable for the cleaving operation which is performed later on.

Next the sample is removed from the glass disc and cleaned. The cleaning procedure involves the use of sulfuric acid-peroxide etch, organic solvents, and deionized water rinse in conjunction with an ultrasonic cleaner. An 80% gold, 20% germanium coating is evaporated on the substrate side and alloyed in a hydrogen atmosphere at about 500°C forming an ohmic contact. The reducing atmosphere is essential in preventing the formation of an oxide layer that destroys the ohmic contact. After this, the aluminum Schottky barrier is evaporated on

the epitaxial layer. Aluminum tends to form an oxide layer in air, so an additional coating of gold is evaporated on top of the aluminum. At this point the sample is cleaved by pressing a knife edge against it. The (110) cleavage planes are perpendicular to the (100) polished face, and the final smaller pieces are rectangular in shape.

Each piece is tested for its suitability as a waveguide modulator. Those that have breakdown at a sufficiently high reverse biasing voltage have their doping profiles measured by the capacitance technique described in Section 3.3. The yield is quite low. About 1% of the barriers sustained 100 volts. This is not too surprising considering the large areas exceeding  $1 \text{ mm}^2$  and the requirements of scrupulous cleanliness in preparing the epitaxial surface before evaporating on the aluminum Schottky barrier.

## 5.2 Modulator Setup

The waveguide modulator described in the last section is mounted on a copper rod that is positioned on the optical bench. The setup for a typical guide is illustrated in Figure XIV. The ohmic contact is silver pasted to the rod, and with the rod grounded, a negative voltage is applied to the Schottky barrier by means of a two mil diameter gold wire pressure contact. The laser beam is focused down to a  $6\text{-}8\mu$  spot incident on a (110) entrance cleavage plane and the guided light distribution is shown as it leaves the exit plane.

Guiding occurs in only the  $x$  direction unless the beam inside the guide spreads enough in  $y$  to hit the outside walls before exiting the guide. Even with guiding in  $x$  and  $y$ , the width along  $y$  is around 100 times the thickness along  $x$ , and the one-dimensional

waveguide theory of the previous chapters is negligibly modified.

This can be shown with the aid of equation 2-21. This is the wave equation for confining TE modes in only the x dimension. If confinement in y is included, we must add a term in y .

$$\frac{\partial^2 E_y}{\partial x^2} + \frac{\partial^2 E_y}{\partial y^2} + [n^2 \frac{\omega^2}{c^2} - \beta^2] E_y = 0 \quad (5-1)$$

Assuming sinusoidal solutions in x and y :

$$\begin{aligned} 0 < x < t & \quad t \sim 10 \\ 0 < y < W & \quad W \sim 1000\mu = 1 \text{ mm} \end{aligned} \quad (5-2)$$

$$E_y(x,y) \sim \sin(hx) \sin(ay)$$

Putting 5-2 into 5-1 we obtain a modified version of equation 2-24 :

$$\beta^2 = n_2^2 \left(\frac{2\pi}{\lambda_0}\right)^2 - h^2 - a^2 \quad (5-3)$$

The terms  $h^2$  and  $a^2$  are proportional respectively to  $1/t^2$  and  $1/W^2$ , so the additional  $a^2$  term makes a change in propagation constant  $\beta^2$  of about  $10^{-4}h^2$  .

Another factor not considered so far is input coupling of the focused laser beam into the guide. Much of the input light does not couple into the discrete guided modes, but leaks into the substrate. This shows up as stray unguided light in the substrate part of the exit plane. The detailed solution of this problem is extremely complicated; however, an idea of how much light is guided can be gained from a ray optics picture.

In Figure XV a light ray is incident at angle  $\theta$  on the epitaxial part of the entrance plane of a waveguide. After entering the guide it glances at angle  $\alpha$  with the substrate interface. If  $\alpha$  is larger than a certain critical angle  $\alpha_c$ , part of the ray's energy leaks into the substrate; and if  $\alpha$  is smaller than  $\alpha_c$ , total internal reflection takes place.

$$n_2 \cos \alpha_c = n_3 \quad (5-4)$$

$$n_2 \sin \alpha_c = \sin \theta_c \quad (5-5)$$

Combining:

$$\sin \theta_c = \sqrt{n_2^2 - n_3^2} \quad (5-6)$$

For small  $\Delta n$  :

$$\theta_c \approx \sqrt{2n_2 \Delta n} \quad (5-7)$$

For typical waveguide numbers:

$$\theta_c \approx 1.5^\circ \quad (5-8)$$

$\theta_c$  can be compared to  $\theta_i$ , the convergence angle of the incoming laser beam.

$$\theta_i \approx \frac{\lambda_0}{s} \quad (5-9)$$

where  $s$  is the focused spot size diameter of the laser beam. For

$s = 7\mu$  :

$$\theta_i \approx 10^\circ \quad (5-10)$$

Thus, in obtaining a small spot size, the laser beam is so sharply focused that a large fraction of the light is lost in the substrate.

### 5.3 Detection Schemes

The infrared light leaving the modulator as shown in Figure XIV is the near field intensity pattern of the guided modes. The output face of the guide is magnified by 100-200X using a microscope objective. The magnified image intensity profile is obtained by means of one of the following three detection schemes:

1. Image Converter
2. Spectrographic Plates
3. Lead Sulfide Detector

The image converter is mainly used for alignment purposes. When a good picture of the output light is obtained, data are acquired by one of the other two methods. The first is the taking of pictures with type Z Kodak spectrographic plates which are sensitive out to  $1.2\mu$ , and the second is the use of a PbS photoconductor detector in conjunction with a light beam chopper and a lock-in amplifier.

The experimental setup using the PbS detector is shown in Figure XVI. A motor driven slit scans the image intensity, and an intensity profile is traced on a strip chart recorder. The intensity is plotted as a function of distance away from the Schottky barrier edge of the modulator's exit plane. The trace contains a peak due to the guided light in the epitaxial layer and a background due to unguided light in the substrate.

The slit is sometimes removed, and the total image intensity is incident on the detector. This is done for polarization measurements. A polarizer is lined up at  $45^\circ$  near the laser so that light incident on the guide is half TE and TM. The output light is sent through an analyzer crossed to the polarizer, and the intensity is measured as a function of the voltage applied to the modulator.

## Chapter 6

### Experimental Results and Interpretations

#### 6.1 Intensity Profiles

The built in refractive index difference between the substrate and the epitaxial layer is so small that only the  $TE_1$  or  $TM_1$  mode can propagate in a passive waveguide. One way of checking this assumption of single mode propagation is by looking at the shapes of the mode profiles on the strip chart recorder.

Positioning of the focused laser beam spot on the entrance plane of the waveguide is crucial in determining the intensity of the guided light. Maximum light intensity is gained when the spot is centered about five microns down from the Schottky barrier edge in the middle of the epitaxial layer. If the spot is off a couple of microns to either side, the guided light intensity drops.

When many modes can propagate, the input spot's location determines the relative amount of the different modes which are excited in the guide. This affects the shape of the intensity profile as well as the overall intensity. However, for single mode propagation there is no longer competition among the different modes, and the shape should remain the same for all input spot positions.

This shape as a function of input spot position is shown in Figure XVII for a 2.8 mm long sample with an epitaxial layer thickness of about  $11\mu$  and a substrate carrier concentration around  $1.5 \times 10^{17} \text{ cm}^{-3}$ . These numbers give a built in index difference about four times above cutoff for the  $TE_1$  or  $TM_1$  mode, and about two times below cutoff for the  $TE_3$  or  $TM_3$  mode.

Referring to Figure XVII, the input beam spot is moved along  $x$  as measured from the Schottky barrier edge of the guide's entrance plane. This makes  $x_c$ , the centered position, about  $5.5\mu$  for maximum overall intensity which is the area under curves (b) and (d). Curves (a) and (c) have greatly different vertical intensity scales as compared to (b). The overall intensity of (b) is over twice that of (a) and ten times that of (c); however, (a), (b), and (c) all have about the same shape indicating that they are probably single mode  $TE_1$ . Passive waveguide theory predicts that the TM curve (d) should have the same shape as the TE curves assuming that all the curves are  $TE_1$  or  $TM_1$  single mode. However, the TE:TM comparison is less satisfactory than the three TE comparisons. None of these comparisons is a conclusive test for single mode propagation, because of the presence of stray unguided light. These data must be combined with additional results to be considered in the rest of Section 6.1 and in Sections 6.2 and 6.3 to establish the presence of single mode light in the waveguide.

Another check on theory and experiment is a comparison of the calculated intensity profiles of Figure XIII with the observed intensity profiles of Figure XVII. The observed profiles correspond to a  $\Delta n$  of about  $4\Delta n_{co}$ . They all have full widths at half maximum between  $5-1/2$  and  $7-1/2\mu$  as compared to the calculated value of  $.68t = 7.5\mu$ . Better agreement between theory and experiment would result from a decrease in  $t$  from  $11$  to  $10\mu$  or an increase in  $N_D$ (substrate) from  $1.5$  to perhaps  $2 \times 10^{17} \text{ cm}^{-3}$ .

The data supplied by Monsanto with the crystal specified a thickness of  $11\mu$  and an  $N_D$ (substrate) of  $1.0 \times 10^{17} \text{ cm}^{-3}$ . This

substrate number gives a  $\Delta n$  of about  $2.5 \Delta n_{CO}$  and poor agreement between observed and calculated full widths at half maximum. As a check, small aluminum dots were evaporated on the substrate, and Schottky barrier measurements yielded a substrate concentration of  $1.5 \times 10^{17} \text{ cm}^{-3} \pm 20\%$ , giving better agreement between measured and theoretical widths of the mode profiles.

The most interesting point of the above discussion is that the experimental widths are actually narrower than the calculated single mode widths. If many modes were excited in the guide, the observed width would be wider tending to give results just the opposite of the above.

One additional point is the predicted similarity between passive guides with and without aluminum coatings. This has been observed. Uncovered guides as long as 6 mm have propagated  $TE_1$  and  $TM_1$  modes with over 50% of the total light energy in the sample contained in the guided mode.

## 6.2 Optical Cutoff Data

The size of the built in index difference between substrate and epitaxial layer necessary for waveguiding was determined by looking at a number of United Aircraft samples with varying substrate concentrations. They all had epitaxial layers with average concentrations between  $.8$  and  $1.5 \times 10^{15} \text{ cm}^{-3}$  and thicknesses between  $9$  and  $13 \mu$ . Three of them are listed below. From each one, many individual modulators were fabricated.

Table II

<u>UAC number</u>	<u><math>N_D</math>(substrate)</u>	<u>Guiding Observed</u>
430A	$8 \times 10^{15}$	No
16A	$23 \times 10^{15}$	No
19B	$45 \times 10^{15}$	Yes

With no applied voltage, the first two did not guide; the last one did. This brackets the value of  $N_D$  for guiding cutoff between  $23 \times 10^{15}$  and  $45 \times 10^{15} \text{ cm}^{-3}$ . The substrate concentrations were derived from Hall effect measurements made by United Aircraft, and are good to about  $\pm 15\%$ . In Section 4.3 the critical (i.e., cutoff) value of  $N_D$  is determined. Equation predicts a value of  $31 \times 10^{15} \text{ cm}^{-3}$  for a 12.5 thick guide which is in agreement with the data of Table II.

The next step is to apply modulation voltages and look at the TE light. Large enough voltages should cause samples 430A and 16A to switch from the non-guiding state through cutoff to a guiding state, and 19B from a guiding to a non-guiding state. In the last case the sign of the index change is reversed.

Table III

<u>Modulator Number</u>	<u><math>N_D</math></u>	<u>V</u>	<u>Goes through cutoff?</u>
430A iii	$8 \times 10^{15}$	150	No
16A vii	$23 \times 10^{15}$	130	Yes
19B i	$45 \times 10^{15}$	75	Yes

The  $TE_1$  intensity profiles for different voltages are shown in Figure XVIII for 16A vii. The transition from no guiding at zero volts to strong guiding at 130 volts is very clear. The doping profile of

16A vii is shown in Figure IX, and the electro-optic model based on it using  $N_D(\text{average}) = 1 \times 10^{15} \text{ cm}^{-3}$  and  $t = 12.5\mu$  in the section on electro-optic switching is in good qualitative agreement with the cutoff data of Figure XVIII.

The opposite transition, from above to below threshold, observed in 19B i is additional support for the electro-optic switching model. Unfortunately, none of the modulators out of sample 19B and others with similar substrate dopings lasted long enough or sustained high enough voltages to obtain good data.

The  $TE_1$  intensity profiles of 16A vii are also photographed on spectrographic plates. Two photographs, one at zero and the other at 130 volts, are shown in Figure XIX. The distinction between guiding and no guiding is unmistakable. The scales measure down from the Schottky barrier edge into the substrate. For  $x > 10\mu$ , unguided light in the substrate is observed. The unguided light undergoes multiple reflections between the top and bottom (100) faces in going through the modulator, and the fringes are caused by interferences between differently reflected light components. The motion up or down of the fringes with applied voltage is useful in determining whether the refractive index of the epitaxial layer is increasing or decreasing with applied voltage. This provides an independent check on the fact that guiding can only be induced with  $\Delta n > 0$ .

This same experiment on 16A vii and other modulators was tried with TM polarized light. In every case, the motion with applied voltage of the fringes is extremely small for the TM light whereas it is large for the TE light. Errors in alignment and local heating

effects at high voltages probably caused the very slight fringe shifts in the TM picture. These observations confirm the electro-optic conclusion yielding  $\Delta n = 0$  for the TM mode.

Finally, we come to modulator 430A iii in Table III which has an  $N_D(\text{substrate})$  of  $8 \times 10^{15} \text{ cm}^{-3}$ . Apparently, this value is so far below cutoff that we do not see waveguiding with applied voltages up to 150 volts.

This presents some difficulties. The linear electrooptic model used in the chapter on the waveguide modulator predicts waveguiding at 150 volts even if the substrate carrier concentration is as low as that of the epitaxial layer. In other words, the index difference generated by the 150 volts is by itself sufficient for waveguiding with  $N_D$  about  $1 \times 10^{15} \text{ cm}^{-3}$ .

Equations 4-9, 4-10, and 4-16 give the fields for the three regions in an electro-optic modulator. With no difference between epitaxial layer and substrate 4-9 and 4-10 are combined into one region.

$$x > w$$

$$E_y(x) \sim e^{-p(x-w)} \quad (6-1)$$

This is done when:

$$C = 0 \quad (6-2)$$

$$-h^2 = p^2 \quad (6-3)$$

$$= 0 \text{ at cutoff}$$

Referring to 4-16, we obtain

$$0 < x < w$$

$$E_1(z) \sim \text{Bi}[-z(0)] \text{Ai}(-z) - \text{Ai}[-z(0)] \text{Bi}(-z) \quad (6-4)$$

$$z(0) = \left(\frac{w}{\Delta}\right)^{2/3} \quad (6-5)$$

$$z(w) = 0 \quad (6-6)$$

Equation 4-20, giving the cutoff condition for the onset of the TE<sub>1</sub> mode, is now simplified.

$$\left. \frac{dE_1}{dz} \right|_{z(w)} = 0 \quad (6-7)$$

This yields

$$Ai'(0) Bi(-z(0)) = Bi'(0) Ai(-z(0)) \quad (6-8)$$

or

$$z(0) = 1.97 \quad (26)$$

hence

$$\begin{aligned} \Delta &= 2n_2 \Delta n_{EO} \left(\frac{2\pi}{\lambda_0}\right)^2 \\ &= \frac{7.63}{w^2} \end{aligned} \quad (6-9)$$

from equations 4-15 and 6-5.

With the following expressions for  $\Delta n_{EO}$  and  $V$

$$\Delta n_{EO} = \frac{1}{2} n_2^3 r_{41} \left(\frac{2V}{w}\right) \quad (6-10)$$

$$V = \frac{N_D e}{2\epsilon} w^2 \quad (6-11)$$

we substitute into 6-9 and obtain cutoff voltage  $V_{co}$  as a function of free carrier concentration  $N_D$ .

$$V_{co} = \frac{N_D^{1/3}}{1360} \quad (6-12)$$

For a carrier concentration of  $10^{15} \text{ cm}^{-3}$  we have

$$V_{co} = 74 \text{ volts} \quad (6-13)$$

Juggling factors like  $r_{41}$  or  $N_D$  by 25% or 50% does not change the result of 6-12 very much. The most likely explanation of the apparent contradiction between 6-13 and the observed data of modulator 430A iii at 150 volts is that it is guiding. However, the guided light intensity is so weak (i.e., the fraction of the input light coupled into the mode is so small) that stray unguided light swamps it out. In order to see the guided light, we must raise  $\Delta n_{EO}$  perhaps 50% above the cutoff value. This corresponds to a 125% increase in  $V$  which is proportional to  $[\Delta n_{EO}]^2$ . Thus, 150 volts for 430A iii, although about two times above the cutoff voltage, is still somewhat below the point where any guided light can be seen.

Using the results just obtained for 430A iii, the data for 16A vii in Figure XVIII can be better understood. Referring to Figure XI, the three index profiles correspond to an epitaxial film with the same thickness  $t$  and the same average  $N_D$  of the epitaxial layer that is measured for 16A vii. Table IV compares cases 2 and 3 in Figure XI and 16A vii.

Table IV

<u>Sample</u>	<u>V (cutoff)</u>	<u><math>N_D</math> (substrate)</u>
Case 2	52	$15 \times 10^{15}$
16A vii	30	$23 \times 10^{15}$
Case 3	0	$31 \times 10^{15}$

Sixty volts was reached before any guided light could be seen in 16A vii. This is twice the cutoff voltage in Table IV, and supports

the conclusions arrived at previously on 430A iii in which no guiding was observed at 150 volts even though it was predicted to occur at 74 volts.

In summary: The phenomena of propagation cutoff in thin optical waveguides is observed. A continuous electro-optic control of the cutoff condition is used to demonstrate its effect on the intensity distribution of the lowest order  $TE_1$  mode.

### 6.3 Intensity Modulation Data

Intensity modulation using an input polarizer at  $45^\circ$  and an output analyzer at  $-45^\circ$  was performed on a 2.4 mm long Monsanto sample with an epitaxial layer thickness near  $11\mu$  and a substrate concentration around  $1.5 \times 10^{17} \text{ cm}^{-3}$  similar to sample 3BY used in Figure XVII for mode profiles.

The output intensity as a function of applied voltage is plotted in Figure XX. The experimental points are closely fitted to

$$I = I_o \sin^2 \frac{\pi}{2} \left( \frac{V-12}{84} \right) \quad (6-14)$$

The minimum is shifted to 12 volts by residual birefringence, and the half wave voltage  $V_{1/2}$  needed to go from a transmission minimum to a maximum is 84 volts. Equation 6-14 is the same as equation 4-67 in Section 4.5 on intensity modulation where

$$\frac{\Gamma}{2} = \frac{\pi}{2} \left( \frac{V-12}{84} \right) \quad (6-15)$$

Two conclusions are reached from the results of Figure XX. First, punch through is obtained at a low modulation voltage; and second, the  $TE_1$  mode changes only a small amount over the entire

voltage range and is nearly the same as the  $TM_1$  mode.

The first conclusion was checked with capacitance measurements which yielded a very small average of  $2 \times 10^{14} \text{ cm}^{-3}$  for the free carrier concentration in the epitaxial layer. As a result, a low punch through voltage of 15 volts was observed. Looking at equation 4-68, the factor  $\eta$  approaches one for strong punch through and  $\Gamma$  becomes proportional to the applied voltage. Keeping in mind the built in birefringence, we have

$$\Gamma = \pi r_{41} n_2^3 \frac{(V-12)L}{\lambda_o t} \quad (6-16)$$

$$\text{Experimental} \quad V_{1/2} = 84 \text{ volts} \quad (6-17)$$

$$\begin{aligned} \text{Calculated} \quad V_{1/2} &= \frac{\lambda_o t}{r_{41} n_2^3 L} \quad (6-18) \\ &= 99 \text{ volts} \end{aligned}$$

This is fairly good agreement considering the uncertainties in  $r_{41}$  and  $t$ .

The shift to a 12 volt minimum improves agreement at higher voltages between the sine squared curve and the experimental points in Figure XX because strong punch through and the behavior associated with it is reached faster, starting from 12 volts than from zero volts. This also explains the asymmetry about  $V = 12$  volts. The experimental points rise faster on the right of the minimum than on the left because of the more rapid rise of  $\Gamma$  at higher voltages where punch through occurs.

The second conclusion of the relative insensitivity of the  $TE_1$  mode to voltage and its similarity to the  $TM_1$  mode was checked in a number of different ways. One test is to remove the analyzer and monitor the intensity  $I_o = I_{xx} + I_{yy}$  as a function of voltage. This was done and  $I_o$  increased by less than 10% in going from zero to 50 volts indicating that the overall  $TE_1$  intensity  $I_{yy}$  rose by less than 20%.

Figures XXI and XXII show the similarities between the  $TE_1$  and  $TM_1$  modes at zero volts and between the  $TE_1$  mode at zero and at 45 volts. The four mode profiles in Figures XXI and XXII each contain about 50% of the total light energy in the guide. Referring to Figure XIII on calculated mode profiles, we are near  $4 \Delta n_{co}$  which gives a calculated full width at half maximum of  $.68t$  which equals  $7.5\mu$  for an  $11\mu$  guide. However, the experimental widths are all between 6 and  $6\frac{1}{2}\mu$  and the same discrepancies between observed and calculated widths seen before in Figure XVII for  $3B\gamma$  occur again for  $3B\beta$ .

In Figure XXII the modulation voltage increases the index in the guide for the  $TE_1$  mode, and the intensity represented by the area under the curve goes up only around 10% from (a) to (b). Such a small increase indicates that the guide at zero volts has to be perhaps four times or more above cutoff or the change from zero to 45 volts would be larger. An interesting feature is the 5% increase in the width at 45 volts. If the guide thickness  $t$  stays constant as the index is raised electro-optically, the mode profile should become slightly narrower along the lines of the profiles shown in Figure XIII. In this case, however, the depletion layer penetrates into the substrate

perhaps a half micron increasing  $t$  and the mode profile width slightly.

Finally, the most convincing test of the equivalence between the  $TE_1$  and  $TM_1$  modes is the ratio of the maximum to minimum intensity of 500 to 1 in Figure XX. Such a huge extinction ratio would not have been possible without a close match between the  $TE_1$  and  $TM_1$  mode profiles. In summary: Intensity modulation has been performed electro-optically in a thin film device with a half wave voltage to go from zero to maximum transmission of less than 100 volts.

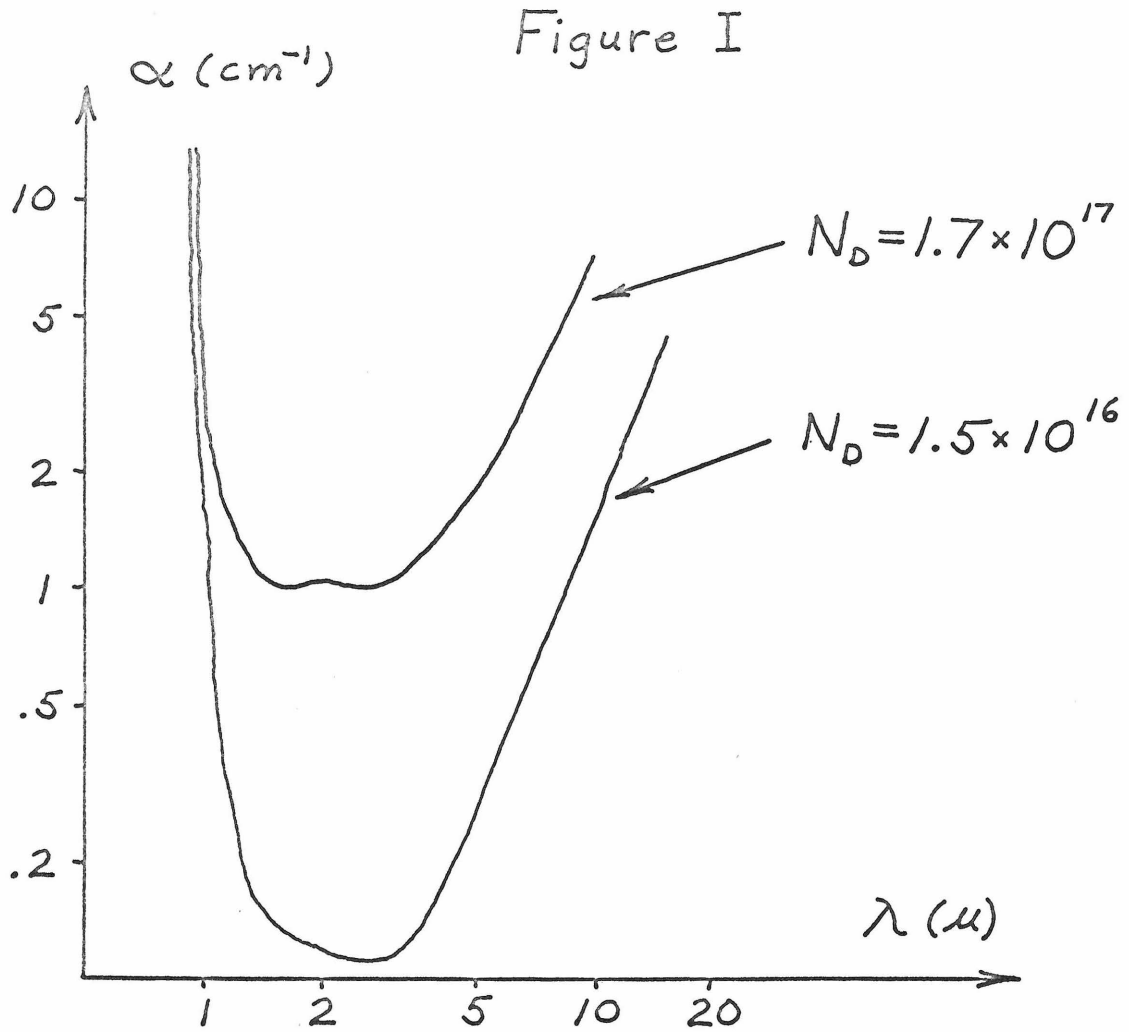
The waveguide modulators described in this section and Section 6.2 use a structure involving an epitaxial layer deposited on a substrate. With this type of structure a number of functions can be envisioned. On a single substrate, coupling, guiding, and modulation can be performed sequentially with metal electrodes applied selectively to certain regions where modulation is to be performed. These operations would all occur on a semiconductor chip with an area of a few square millimeters. This description gives an idea of the possibilities in the new field of integrated optics in which optical elements on a single substrate will replace the present day optical circuits consisting of isolated components (lenses, polarizers, modulators) all mounted on an optical bench.

Figure Captions

- Fig. I Infrared absorption in n-type GaAs.
- Fig. II Refractive index of GaAs.
- Fig. III Waveguide configuration and index profile of passive waveguide.
- Fig. IV Graphical solutions to the guided modes.
- Fig. V Four lowest order modes of symmetric dielectric waveguide.
- Fig. VI Schottky barrier under no voltage bias.
- Fig. VII Schottky barrier under reverse biasing voltage.
- Fig. VIII Voltage vs.  $1/C^2$  for a Schottky barrier.
- Fig. IX Space charge concentration vs. depletion layer width.
- Fig. X Electrooptic modulator configuration and index profile.
- Fig. XI Three index profiles for the  $TE_1$  mode at cutoff.
- Fig. XII Electric field and space charge profiles.
- Fig. XIII Four  $TE_1$  ( $TM_1$ ) intensity profiles as a function of  $\Delta n$  in a passive waveguide.
- Fig. XIV Mounted waveguide modulator.
- Fig. XV Light ray inside modulator.
- Fig. XVI Experimental setup.
- Fig. XVII Intensity profiles of passive waveguide 3BY.
- Fig. XVIII Intensity profiles of  $TE_1$  mode at different applied voltage for 16A vii.
- Fig. XIX  $TE_1$  mode photographs at zero and 130 volts for 16A vii.
- Fig. XX Transmittance of  $3b\beta$  between crossed polarizers as a function of applied voltage.

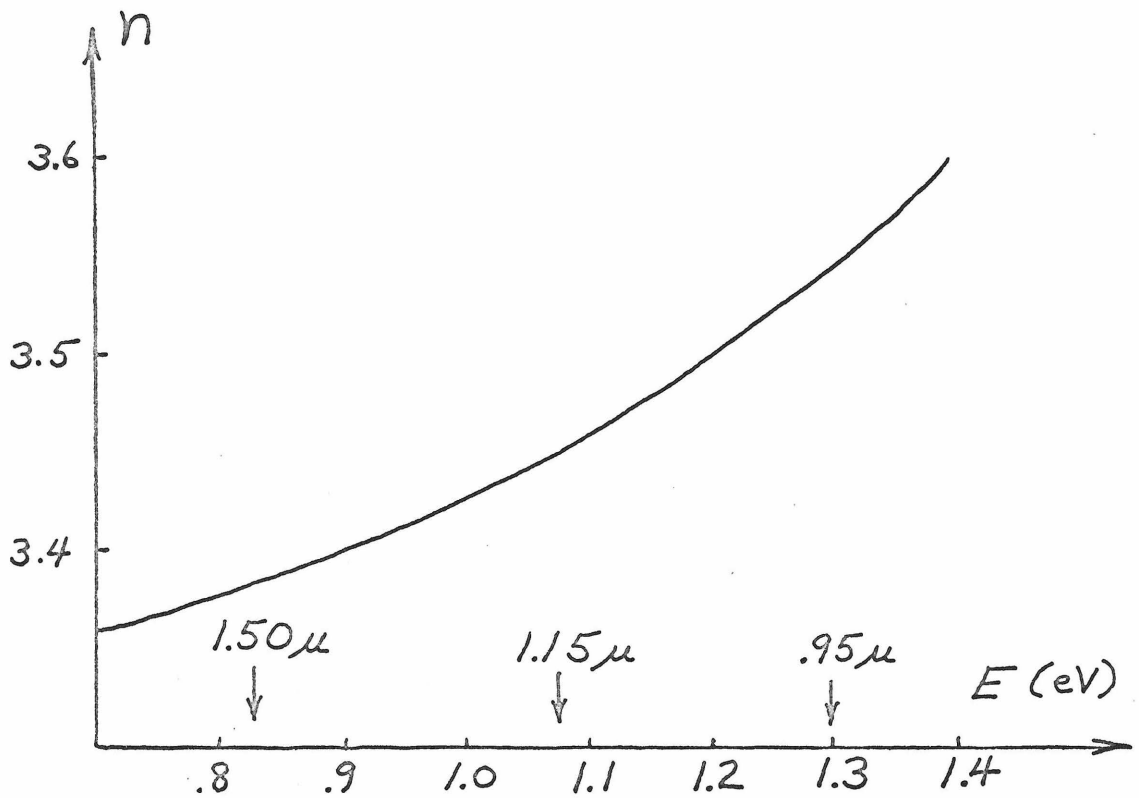
Fig. XXI  $TE_1$  and  $TM_1$  intensity profiles at zero volts for  $3B\beta$ .

Fig. XXII  $TE_1$  intensity profile at zero and 45 volts for  $3B\beta$ .



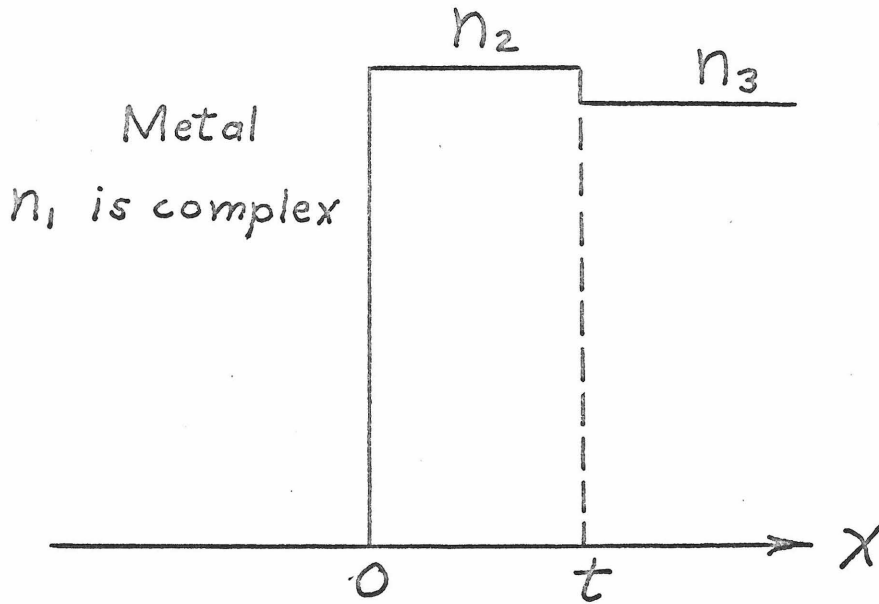
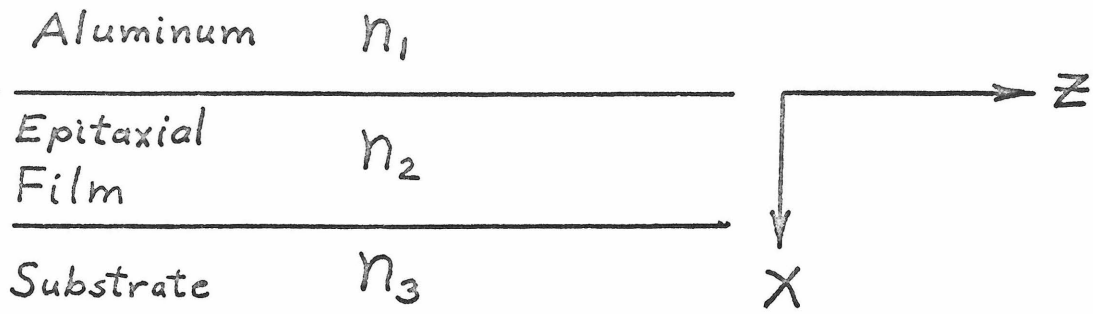
Absorption in n-type GaAs  
as a function of wavelength  
at  $T = 300^\circ\text{K}$  (from ref. 12)

Figure II



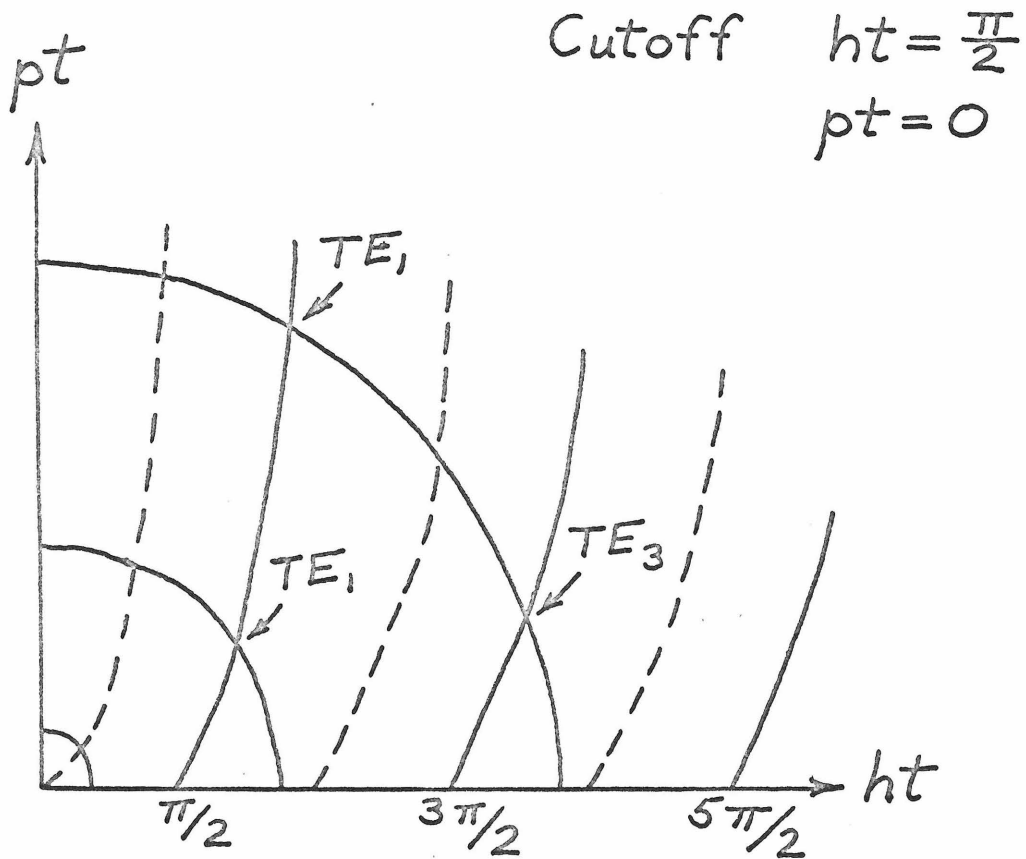
Refractive Index of GaAs.  
as a function of photon energy  
near the absorption edge  
at  $T=300^\circ\text{K}$  (from ref. 15)

Figure III



Waveguide Configuration and Index Profile for Epitaxial Film between Aluminum and Substrate

Figure IV

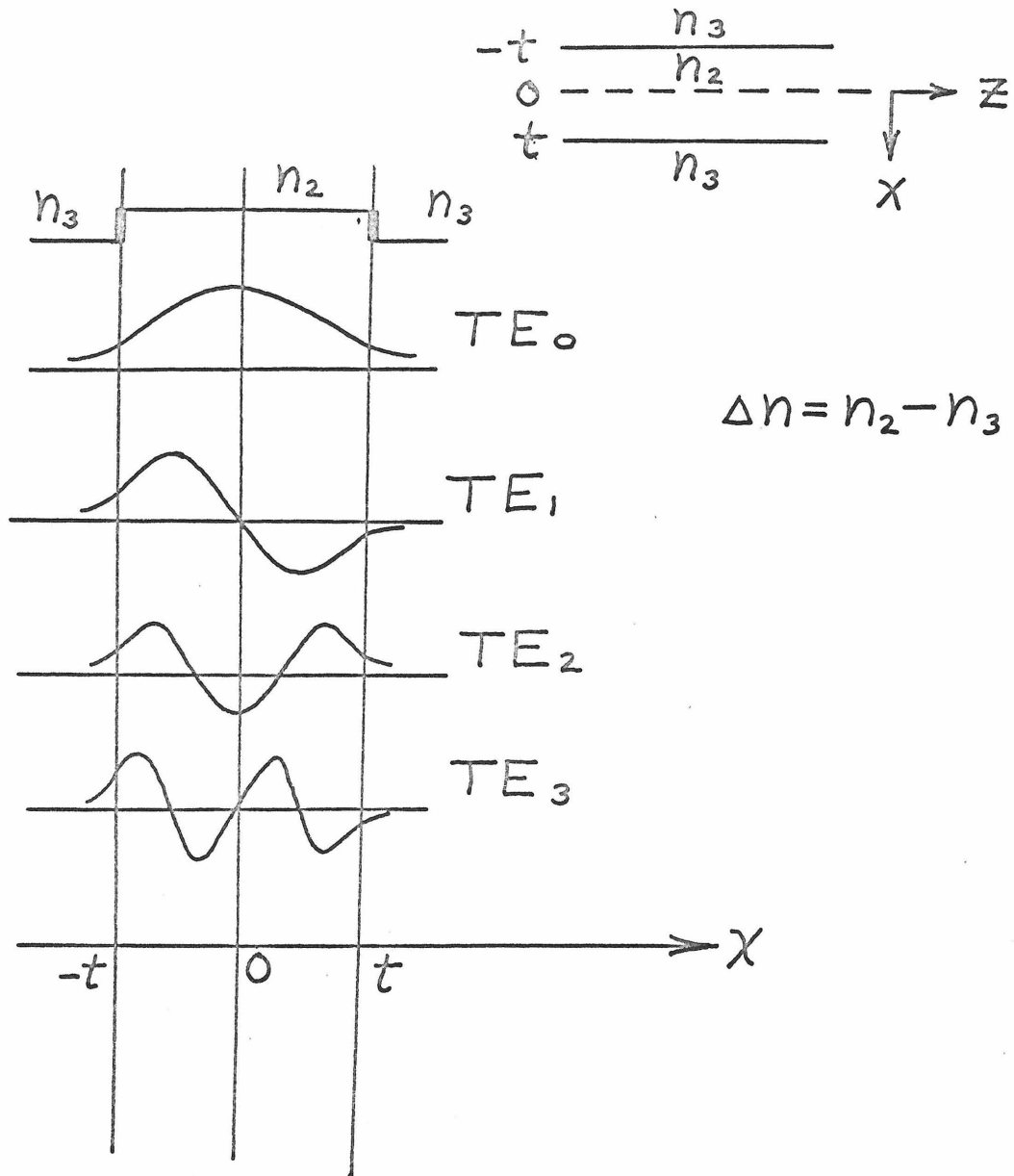


$$(ht)^2 + (pt)^2 = 2n_2\Delta n \left(\frac{2\pi}{\lambda_0}\right)^2 t^2$$

$$pt = -ht \cot(ht)$$

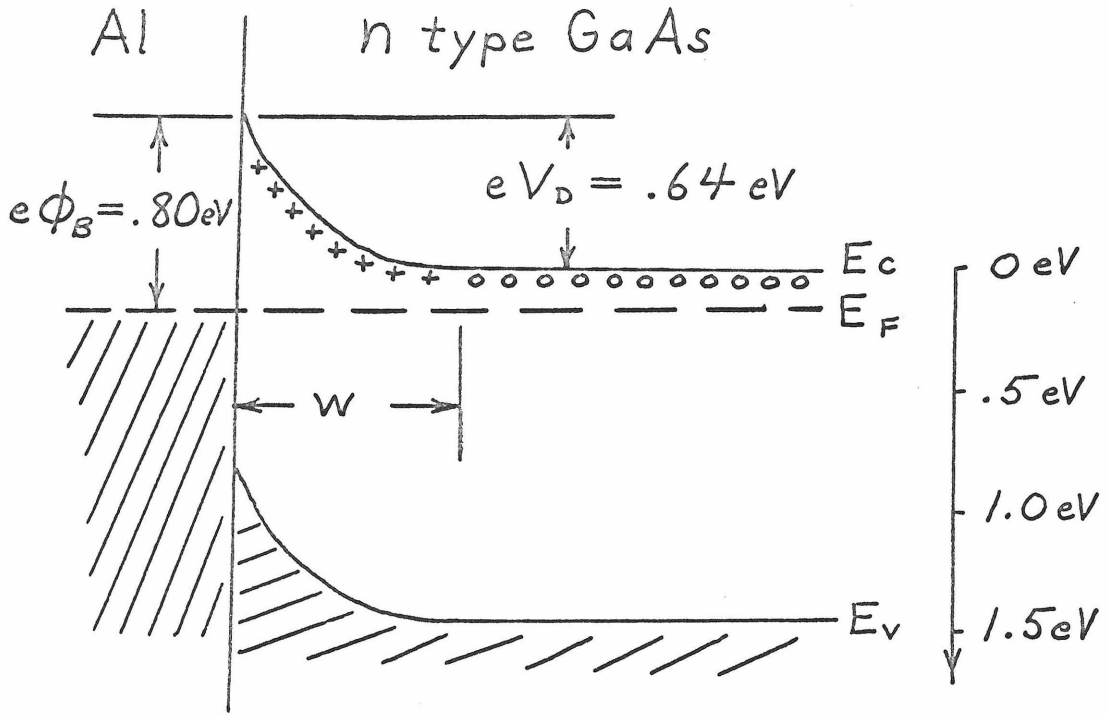
Graphical  
Solutions to the guided  
modes (TE and TM)

Figure V



Four lowest order modes of  
symmetric dielectric waveguide  
TE or TM

Figure VI



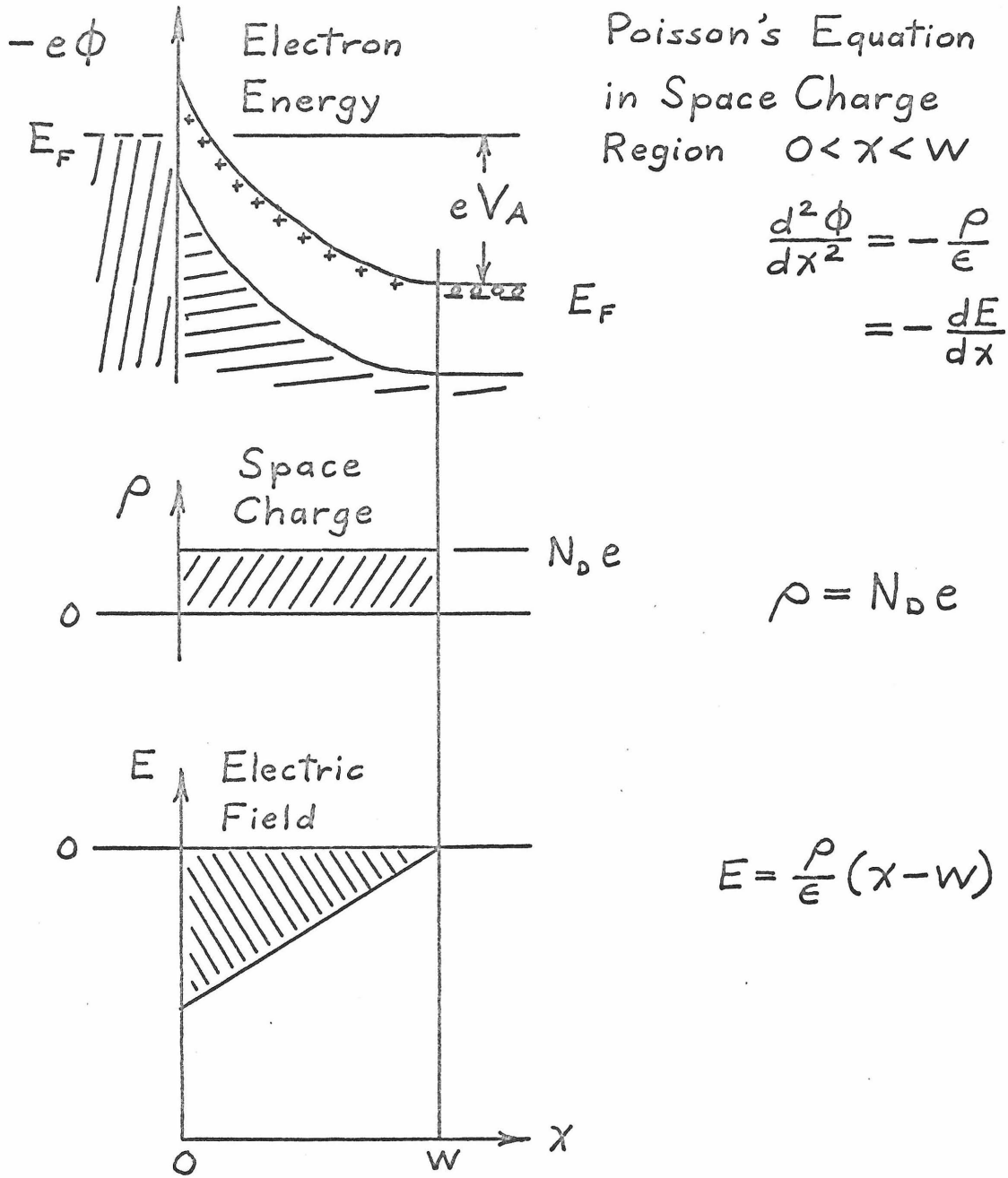
$$E_G = E_c - E_v = 1.43\text{ eV}$$

$$N_D = 10^{15}\text{ cm}^{-3}$$

$$E_c - E_F = .16\text{ eV}$$

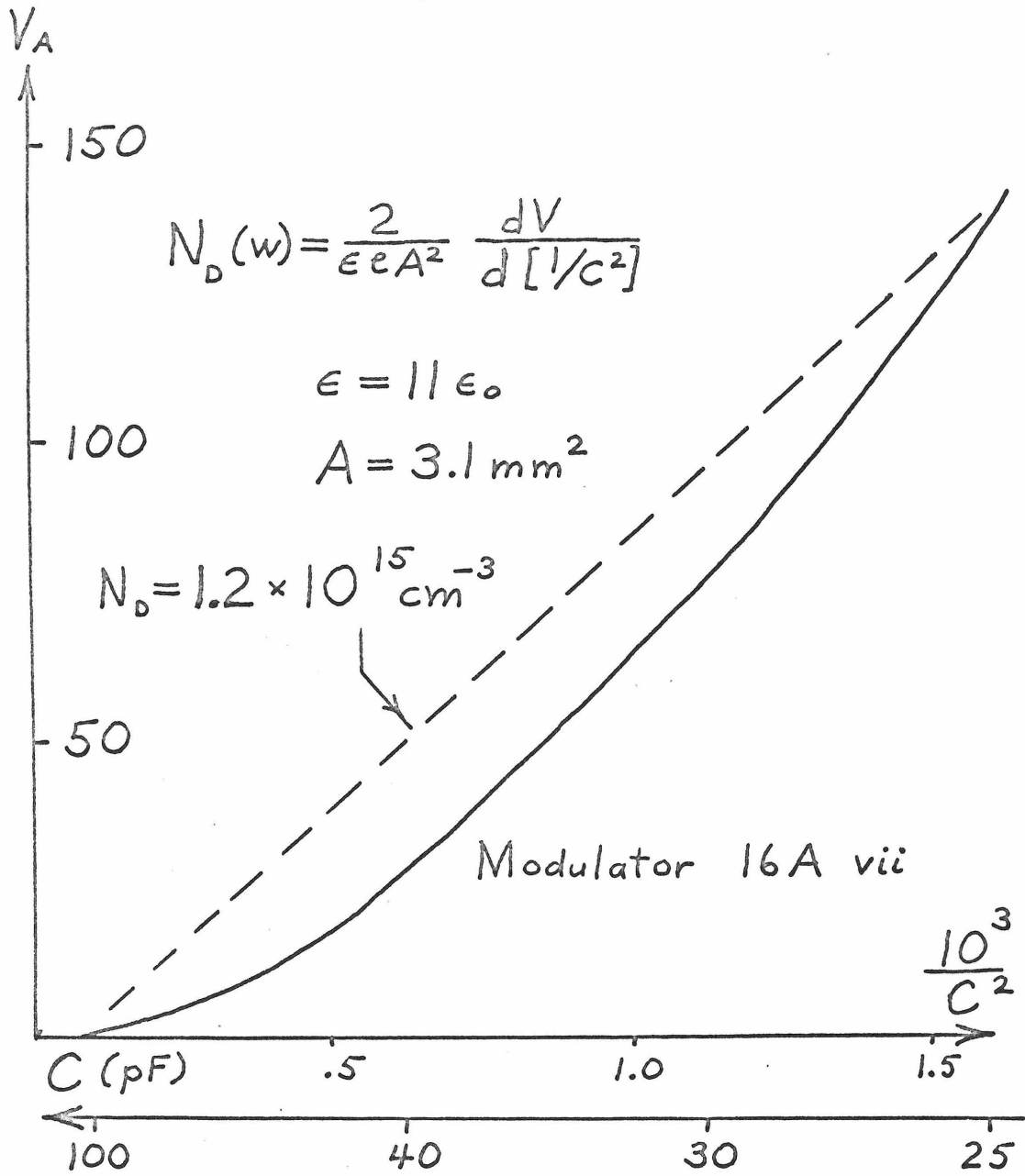
Schottky Barrier under  
No Biasing Voltage

Figure VII



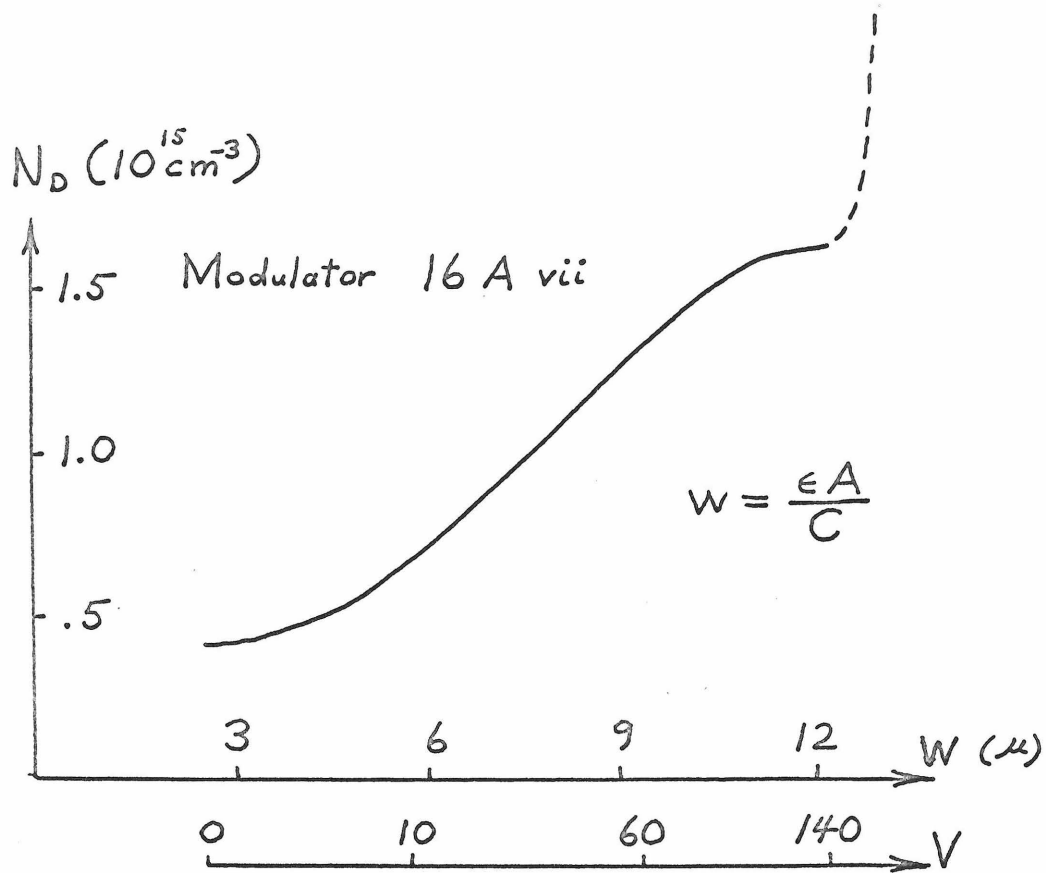
Schottky Barrier under Reverse Biasing Voltage

Figure VIII



Applied Voltage as a Function of  $\frac{1}{C^2}$   
for a Schottky Barrier

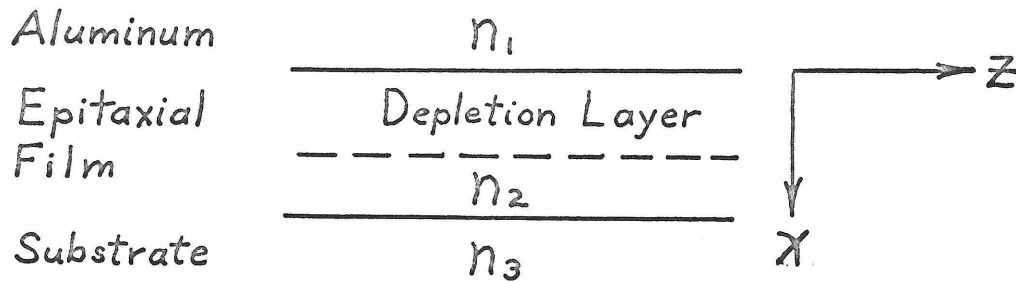
Figure IX



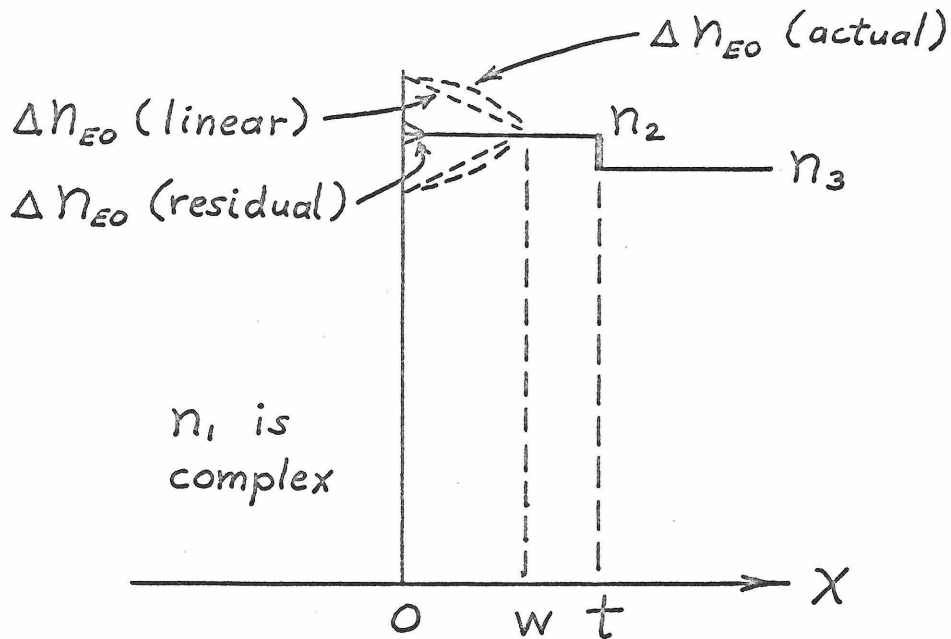
$N_D(w)$  as a function of  $w$  is derived from the data of figure VIII.

Space Charge Concentration  
as a Function of  
Depletion Layer Width

Figure X



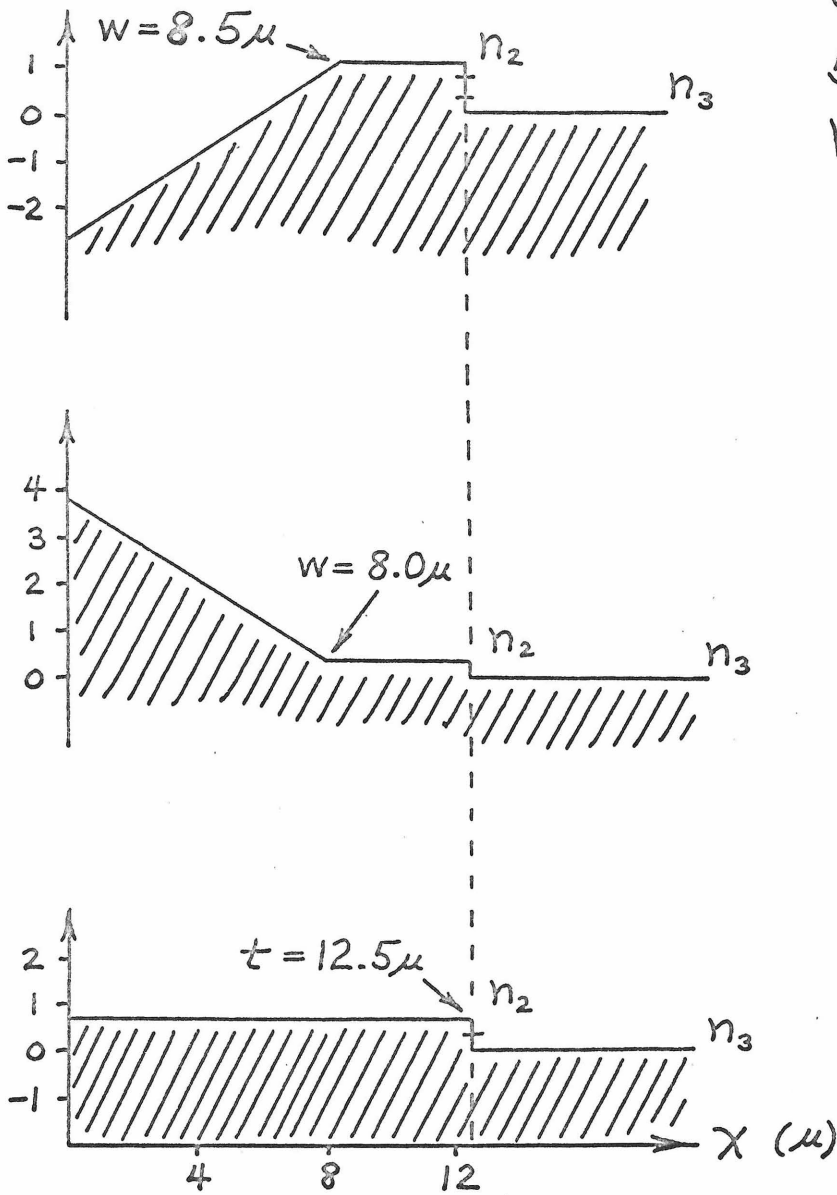
$z$  is either in the  $[011]$  or  $[01\bar{1}]$  direction



Electrooptic Modulator Configuration and Index Profile

Figure XI

$\Delta n$  (units of  $10^{-4}$ )



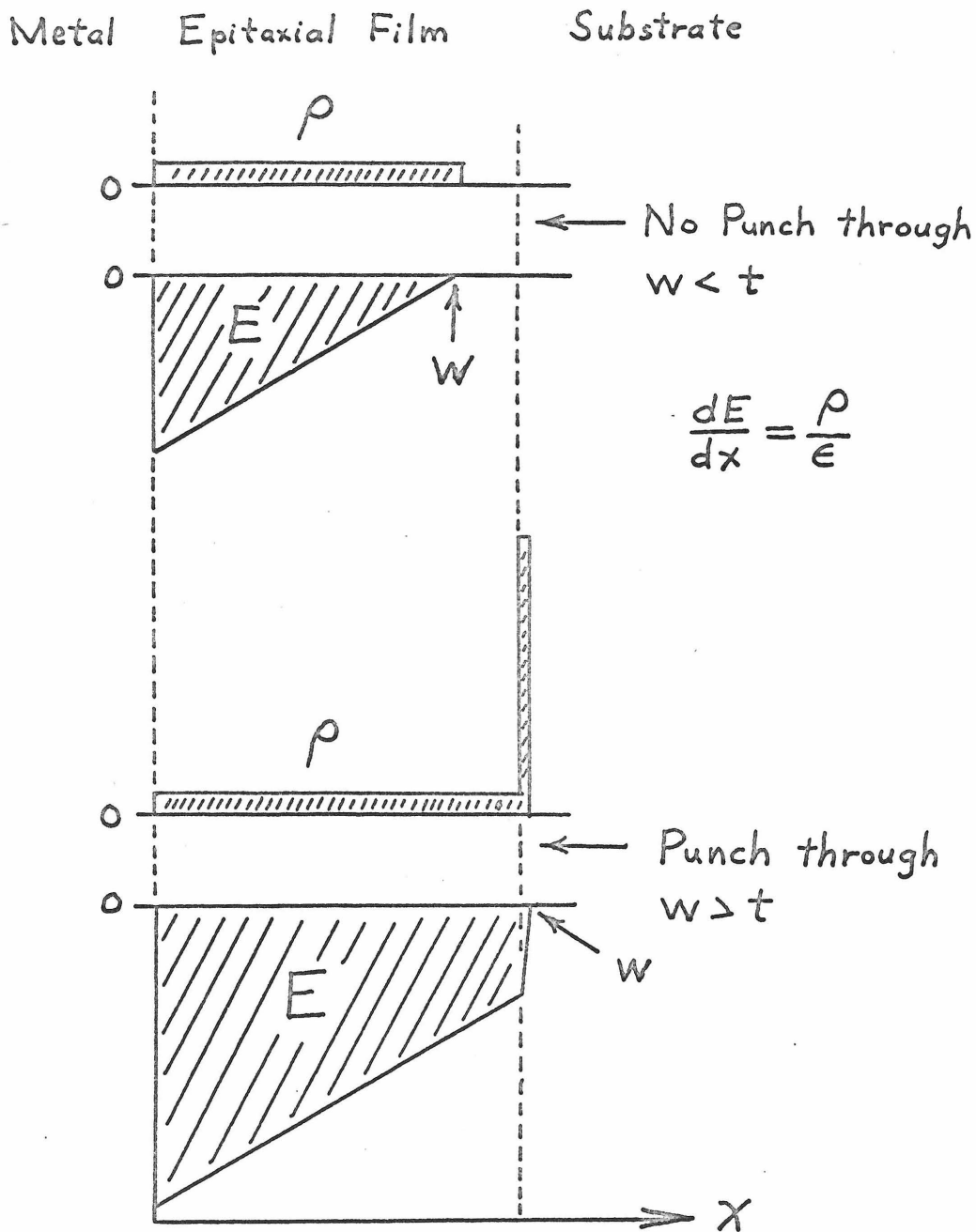
Case 1  
50% above  
 $V_{co} = 60v$

Case 2  
50% below  
 $V_{co} = 52v$

Case 3  
 $V_{co} = 0v$

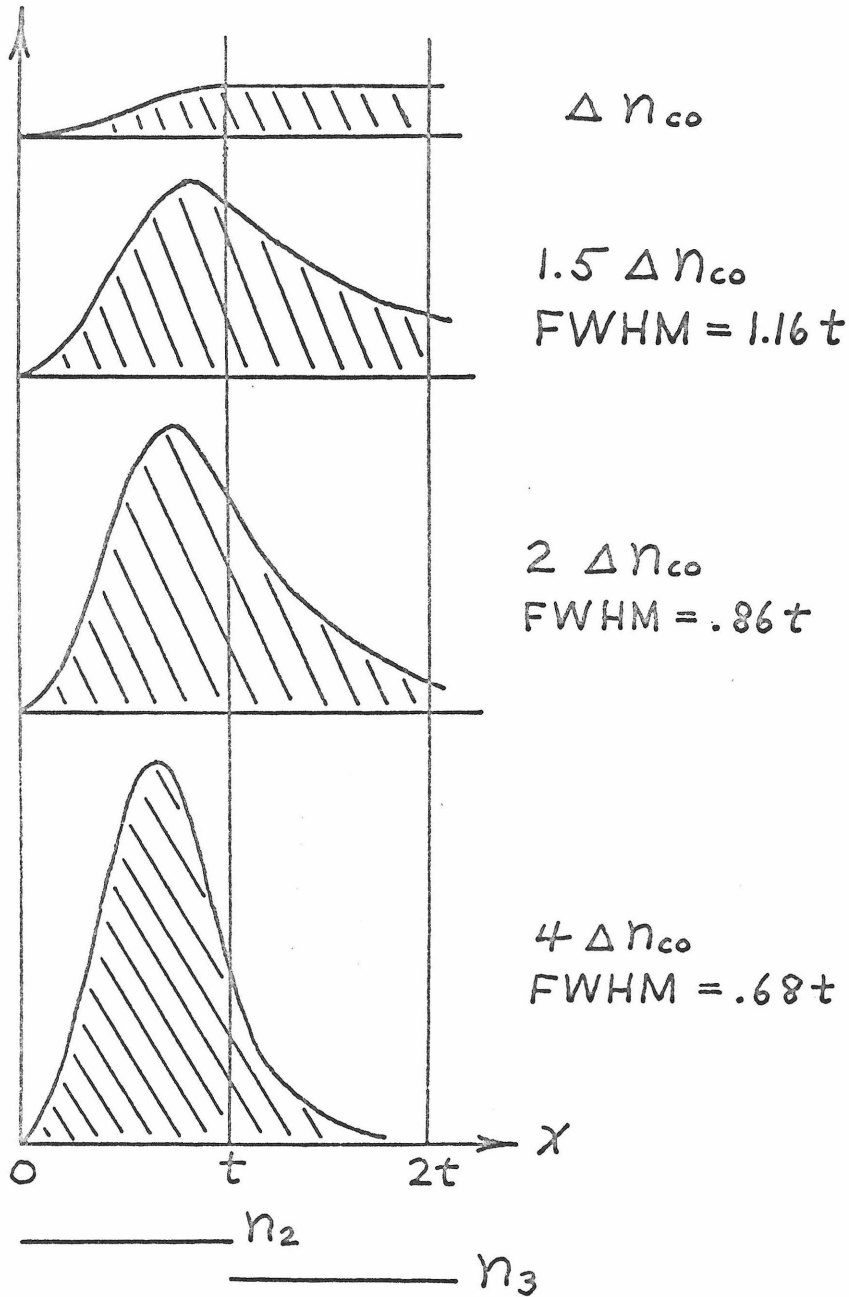
Three Index Profiles for  
the  $TE_1$  Mode at Cutoff

Figure XII



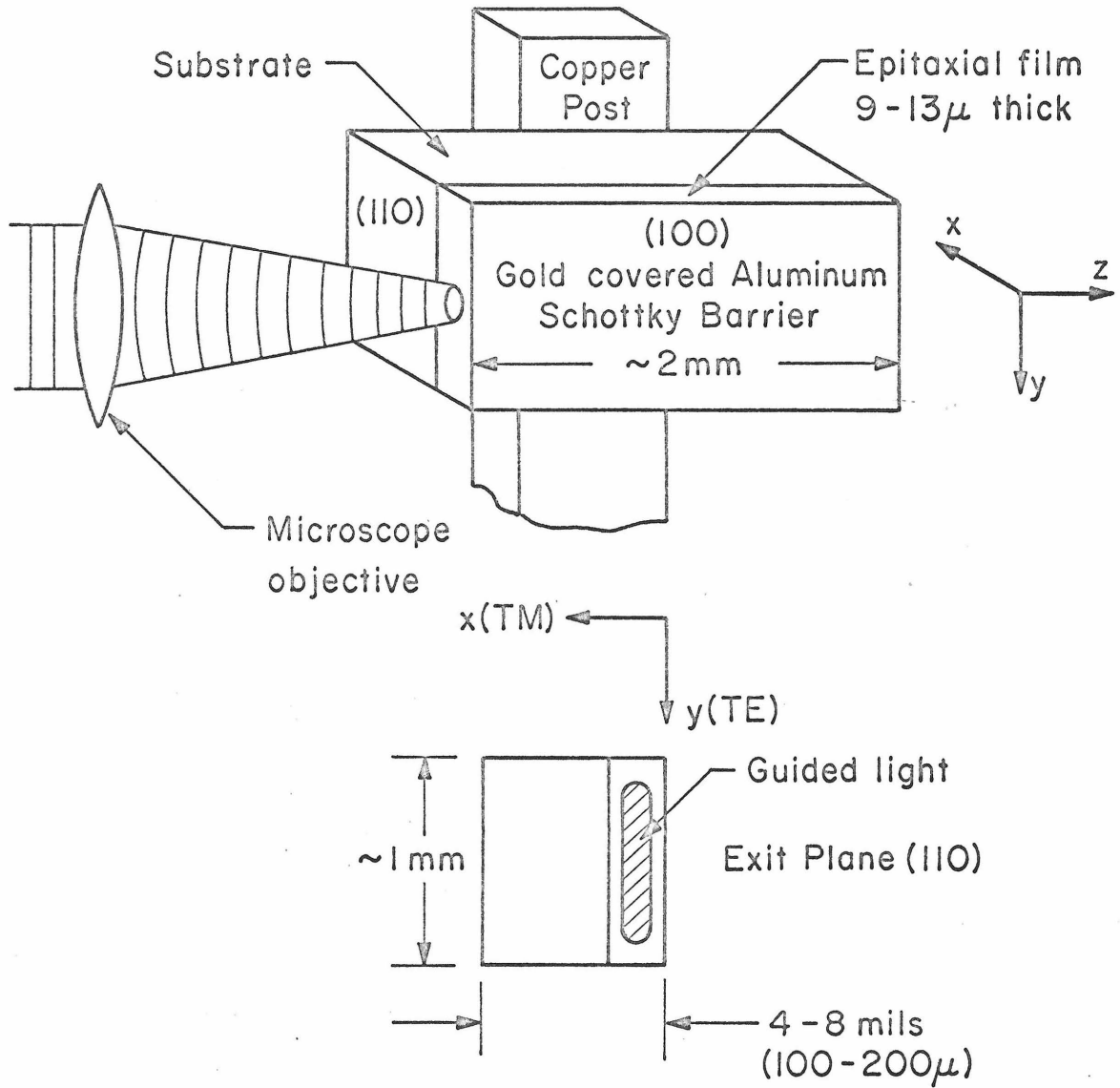
Electric Field and  
Space Charge Profiles

Figure XIII



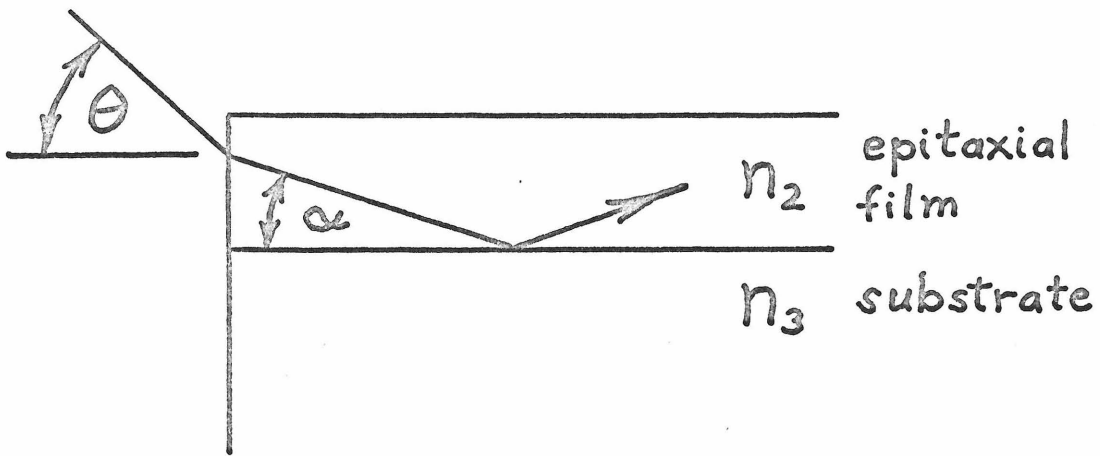
Four  $TE_1$  ( $TM_1$ ) Intensity Profiles  
as a function of  $\Delta n$  in a Passive Waveguide

Figure XIV



Mounted Waveguide Modulator

Figure XV



$$\lambda_0 = 1.15\mu$$

$$n_2 = 3.45$$

$$\Delta n = n_2 - n_3 = 10^{-4}$$

Light Ray inside Modulator

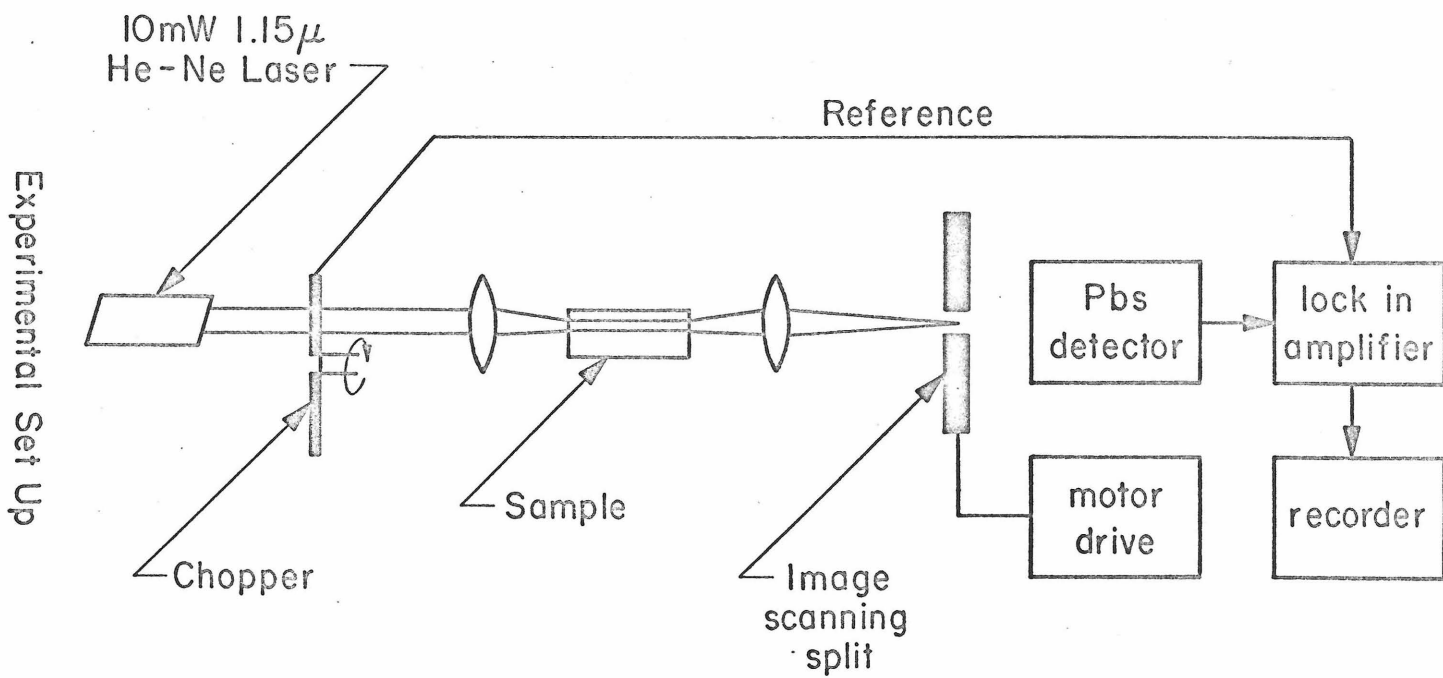
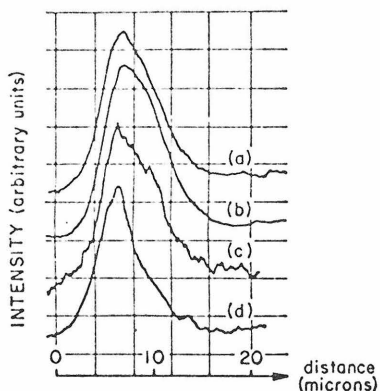


Figure XVI

Figure XVII



Distance measured  
from Schottky  
barrier edge in  
toward substrate

Monsanto

Sample 3B $\gamma$

$$L = 2.8 \text{ mm}$$

$$N_D(\text{substrate}) = 1.5 \times 10^{17}$$

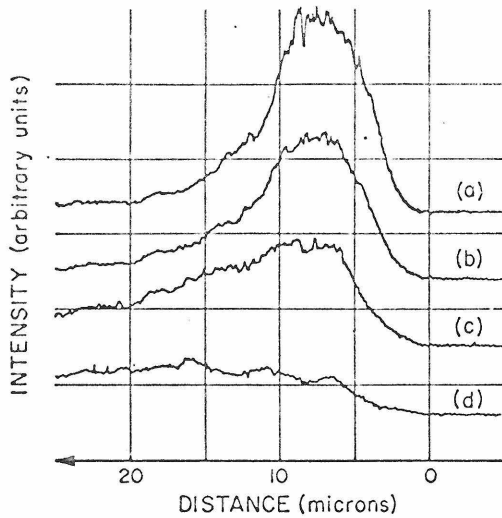
$$t = 11 \mu$$

$$x_c \sim \frac{t}{2}$$

Mode	Input Beam Position ( $\mu$ )
(a) TE	$x_c + 5$
(b) TE	$x_c$
(c) TE	$x_c - 5$
(d) TM	$x_c$

Intensity Profiles  
of Passive Waveguide

Figure XVIII



Same intensity scale for each of the intensity profiles.

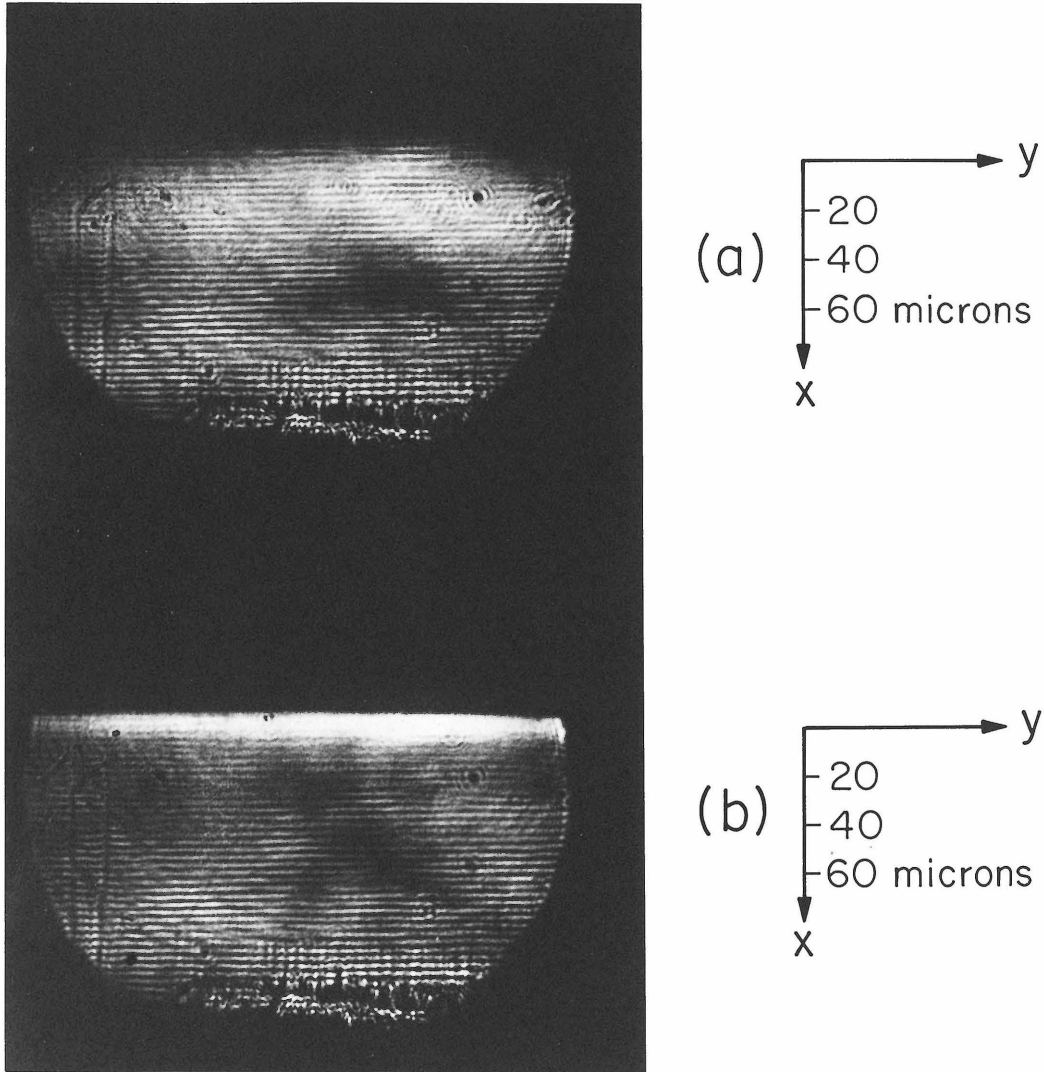
United Aircraft Sample 16A vii

Voltages

(a)	130	$L = 2.3 \text{ mm}$
(b)	100	$t = 12.5 \mu$
(c)	70	$N_0(\text{substrate}) = 23 \times 10^{15} \text{ cm}^{-3}$
(d)	0	

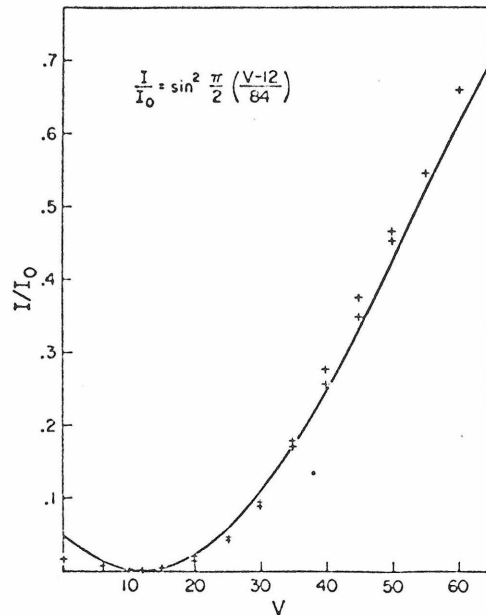
Intensity Profiles of TE<sub>1</sub> Mode  
at different applied voltages

# Figure XIX



Sample 16A vii  
TE<sub>1</sub> Mode Photographs at  
zero volts (a) and 130 volts (b)

Figure XX



Monsanto

Sample 3B B

$$L = 2.4 \text{ mm}$$

$$t \approx 11 \mu$$

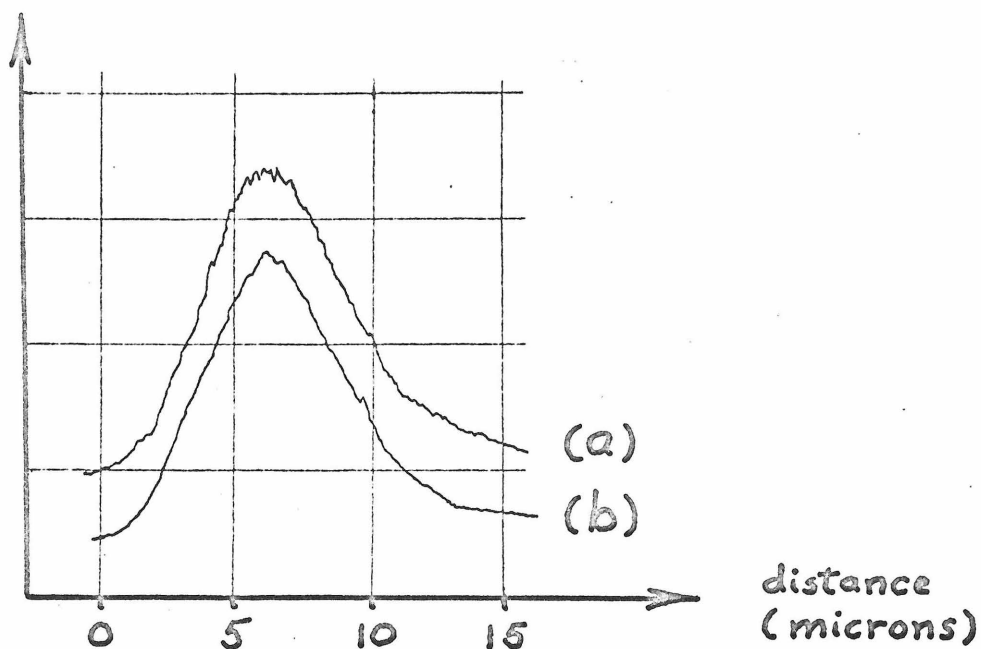
$$N_0 (\text{substrate}) \approx 1.5 \times 10^{17}$$

Transmittance of Waveguide  
between crossed polarizers as a  
function of applied voltage

# Figure XXI

Monsanto Sample 3B $\beta$

Intensity  
(arbitrary units)



(a)  $TM_1$       FWHM =  $6.0\mu$

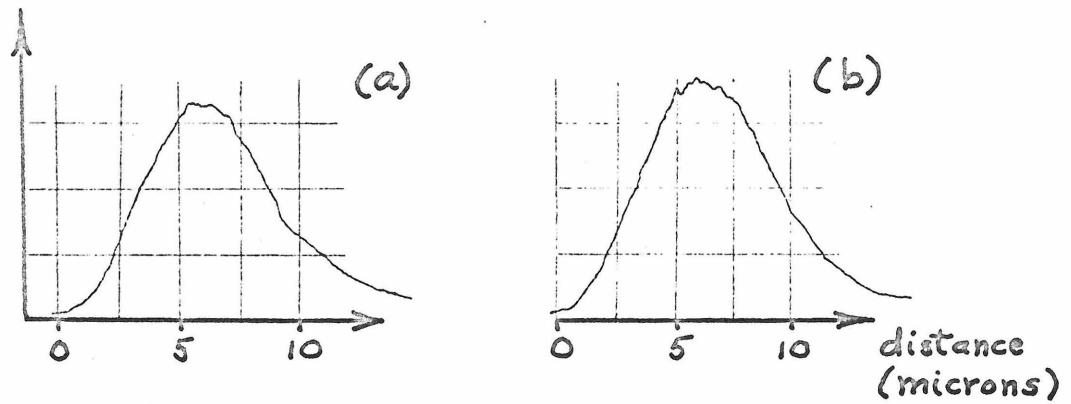
(b)  $TE_1$       FWHM =  $6.1\mu$

$TE_1$  and  $TM_1$  Intensity  
Profiles at Zero Volts

Figure XXII

Monsanto Sample 3BB

Intensity  
(arbitrary units)



- |     |                 |          |              |
|-----|-----------------|----------|--------------|
| (a) | TE <sub>1</sub> | 0 volts  | FWHM = 6.1 μ |
| (b) | TE <sub>1</sub> | 45 volts | FWHM = 6.4 μ |

TE<sub>1</sub> Intensity Profiles at  
Zero and 45 Volts

References

1. P.K. Tien, R. Ulrich, and R.J. Martin, "Modes of Propagating Light Waves in Thin Deposited Semiconductor Films," Appl. Phys. Letters 14, 291 (1969).
2. M.L. Dakss, L. Kuhn, P.F. Heidrich, and B.A. Scott, "Grating Coupler for Efficient Excitation of Optical Guided Waves in Thin Films," Appl. Phys. Letters 16, 523 (1970).
3. F. Chen, "Modulators for Optical Communications," Proc. IEEE 58, 1440 (1970).
4. D.F. Nelson and F.K. Reinhart, "Light Modulation by the Electro-optic Effect in Reverse Biased GaP P-N Junctions," Appl. Phys. Letters 5, 148 (1964).
5. W.L. Walters, "Electrooptic Effect in Reverse Biased GaAs P-N Junctions," J.A.P. 37, 916 (1966).
6. F.K. Reinhart, D.F. Nelson, and J. McKenna, "Electrooptic and Waveguide Properties of Reverse Biased GaP P-N Junctions," Phys. Rev. 117, 1208 (1969).
7. D. Hall, A. Yariv, and E. Garmire, "Optical Guiding and Electro-optic Modulation in GaAs Epitaxial Layers," Optics Communications 1, 403 (1970).
8. D. Hall, A. Yariv, and E. Garmire, "Observation of Propagation Cutoff and Its Control in Thin Optical Waveguides," Appl. Phys. Letters 17, 127 (1970).
9. S.M. Sze, Physics of Semiconductor Devices, Wiley and Sons, 1969.

10. J.S. Harris, Y. Nannichi, G.L. Pearson, and G.F. Day, "Ohmic Contacts to Solution Grown GaAs," J.A.P. 40, 4575 (1969).
11. W. Cochran, S.J. Fray, F.A. Johnson, J.E. Quarrington, and N. Williams, "Lattice Absorption in GaAs," J.A.P. 35, 2102 (1961).
12. M.G. Mil'vidskii, V.B. Osvenskii, E.P. Rashevskaya, and T.G. Yugova, "Investigation of the Infrared Absorption Spectrum of n-type GaAs," Soviet Physics - Solid State 7, 2784 (1966).
13. W.G. Spitzer and J.M. Whelan, "Infrared Absorption and Electron Effective Mass in n-type GaAs," Phys. Rev. 114, 59 (1959).
14. C.E. Jones, Jr. and A.R. Hilton, "Optical Absorption in Chromium Doped, High Resistivity GaAs in the .6 to 1.5 eV Range," J. Electrochem. Soc. 113, 503 (1966).
15. D.T.F. Marple, "Refractive Index of GaAs," J.A.P. 35 1241 (1964).
16. T.S. Moss, Optical Properties of Semiconductors, Academic Press, 1961.
17. F. Stern, "Dispersion of the Index of Refraction Near the Absorption Edge of Semiconductors," Phys. Rev. 133, A1653 (1964).
18. A. Yariv, Quantum Electronics, Wiley and Sons, 1967.
19. L. Ho and C.F. Buhrer, "Electrooptic Effect of GaAs," Appl. Opt. 2, 647 (1963).
20. I.P. Kaminow and E.H. Turner, "Electrooptic Effect in GaAs," J. Opt. Soc. Am. 53, 523 (1963).
21. K.S. Viswanathan and J. Callaway, "Dielectric Constant of a Semiconductor in an External Electric Field," Phys. Rev. 143, 564 (1966).
22. T.S. Moss, "Optical Absorption Edge in GaAs and its Dependence on Electric Field," J.A.P. 32, 2136 (1961).

23. V. Bagaev, Y. Berozashvili, and L. Keldysh, "Electrooptical Effect in GaAs," J.E.T.P. Letters 4, 364 (1966).
24. R.P. Feynman, R.B. Leighton, and M. Sands, Lectures on Physics, Vol. II, Addison Wesley, 1964.
25. G. Hass, Applied Optics and Optical Engineering, Vol. III, ed. by R. Kingslake, Academic Press (1965).
26. R.E. Collin, Field Theory of Guided Waves, McGraw Hill, 1960.
27. J. Bardeen, "Surface States and Rectification at a Metal-Semiconductor Contact," Phys. Rev. 71, 717 (1947).
28. V. Heine, "Theory of Surface States," Phys. Rev. 138, A1689 (1965).
29. C.A. Mead, "Metal-Semiconductor Surface Barriers," Solid State Electronics 9, 1023 (1966).
30. D. Kahng, "Conduction Properties of the Au-n type Si Schottky Barrier," Solid State Electronics 6, 281 (1963).
31. N.I. Meyer and T. Gulbrandsen, "Method for Measuring Impurity Distributions in Semiconductor Crystals," Proc. IEEE 51, 1631 (1963).
32. D. Kahng, "Au-n-type GaAs Schottky Barrier and its Varactor Application," Bell Sys. Tech. J. 43, 215 (1964).
33. H.A. Antosiewicz, Handbook of Mathematical Functions 10.4, ed. by M. Abramowitz and I. A. Stegun, National Bureau of Standards (1965).